THE ASTROPHYSICAL JOURNAL, 519:802–833, 1999 July 10

DWARFS COOLER THAN "M": THE DEFINITION OF SPECTRAL TYPE "L" USING DISCOVERIES FROM THE 2-MICRON ALL-SKY SURVEY (2MASS)[1]

J. DAVY KIRKPATRICK
Infrared Processing and Analysis Center, MS 100-22, California Institute of Technology, Pasadena, CA 91125; davy@ipac.caltech.edu
I. NEILL REID
Palomar Observatory, MS 105-24, California Institute of Technology, Pasadena, CA 91125
JAMES LIEBERT
Steward Observatory, University of Arizona, Tucson, AZ 85721
ROC M. CUTRI, BRANT NELSON, AND CHARLES A. BEICHMAN
Infrared Processing and Analysis Center, MS 100-22, California Institute of Technology, Pasadena, CA 91125
CONARD C. DAHN AND DAVID G. MONET
US Naval Observatory, P.O. Box 1149, Flagstaff, AZ 86002
AND
JOHN E. GIZIS AND MICHAEL F. SKRUTSKIE
Five College Astronomy Department, Department of Physics and Astronomy, University of Massachusetts, Amherst, MA 01003
Received 1998 November 30; accepted 1999 February 16

ABSTRACT

Before the 2-Micron All-Sky Survey (2MASS) began, only six objects were known with spectral types later than M9.5 V. In the first 371 deg^2 of actual 2MASS survey data, we have identified another 20 such objects spectroscopically confirmed using the Low Resolution Imaging Spectrograph (LRIS) at the W. M. Keck Observatory. Because the TiO and VO bands, which dominate the far-optical portions of late-M spectra, disappear in these cooler dwarfs, we define a new spectral class "L" in which metallic oxides are replaced by metallic hydrides and neutral alkali metals as the major spectroscopic signatures. We establish classification indices and type all 25 L dwarfs. The 26th "post-M9.5" object—Gl 229B—is the prototype of a methane-dominated spectral class, which we propose as class "T." At least five of the 20 2MASS L dwarfs show the 6708 Å lithium doublet at low resolution, the strongest having an equivalent width of 18.5 Å. For objects this cool, the presence of lithium proves that they are substellar. Two other 2MASS objects appear to have lithium lines at the limit of our detectability, which if verified means that at least one-third of our L dwarfs are bona fide brown dwarfs. All of the 2MASS brown dwarfs discovered so far have $J-K_s>1.30$. We have not yet, despite deliberately searching for them, found any brown dwarfs with colors resembling Gl 229B ($J-K_s\approx -0.1$).

Subject headings: infrared: stars — stars: atmospheres — stars: distances — stars: fundamental parameters — stars: low-mass, brown dwarfs

1. INTRODUCTION

Near-infrared sky surveys have the potential to reveal more stars in the solar neighborhood—particularly those missed in proper-motion searches and those near the bottom of the main sequence. It is expected that such surveys might find stellar objects cooler than those known from optical surveys or even find nearby brown dwarfs. Indeed, follow-up of initial point sources discovered from the 2-Micron All-Sky Survey (2MASS) Prototype Cameras and the Deep Near-Infrared Sky (DENIS) survey uncovered several objects with spectral types later than M9.5 V, the end of the M-dwarf sequence (Kirkpatrick, Beichman, & Skrutskie 1997a; Delfosse et al. 1997). These results suggested that a more systematic search of an early subset of 2MASS survey data might discover a substantial number of these objects.

In this paper, we report the successful results of just such an endeavor covering 371 deg^2 and including 66 candidate objects. We outline in § 2 the target selection process used on a subset of initial survey data and discuss in § 3 the follow-up spectroscopy. Observed 2MASS counterparts—plus several similar objects pulled from the literature—showing spectra later in type than M9.5 V are discussed and displayed in § 4, where the case is made for establishing a new spectral class. In § 5 we present the complete definition of this new spectral class, which we will call "L." In § 6, two key clues to the mass and age of the L dwarfs—Hα line strength and lithium detection—are discussed along with other line strengths and colors. Trigonometric parallaxes for a few of the L dwarfs are presented in § 7. In § 8, the atmospheric physics and temperature scale of L dwarfs are discussed. Results are summarized in § 9.

2. TARGET SELECTION

To search for objects cooler than the coolest known stars, we must choose color criteria that exclude the majority of M dwarfs and other main sequence stars but that include objects like the brown dwarf candidate GD 165B ($J-K=1.58$) and the methane brown dwarf Gl 229B

[1] Portions of the data presented herein were obtained at the W. M. Keck Observatory, which is operated as a scientific partnership among the California Institute of Technology, the University of California, and the National Aeronautics and Space Administration. The Observatory was made possible by the generous financial support of the W. M. Keck Foundation.

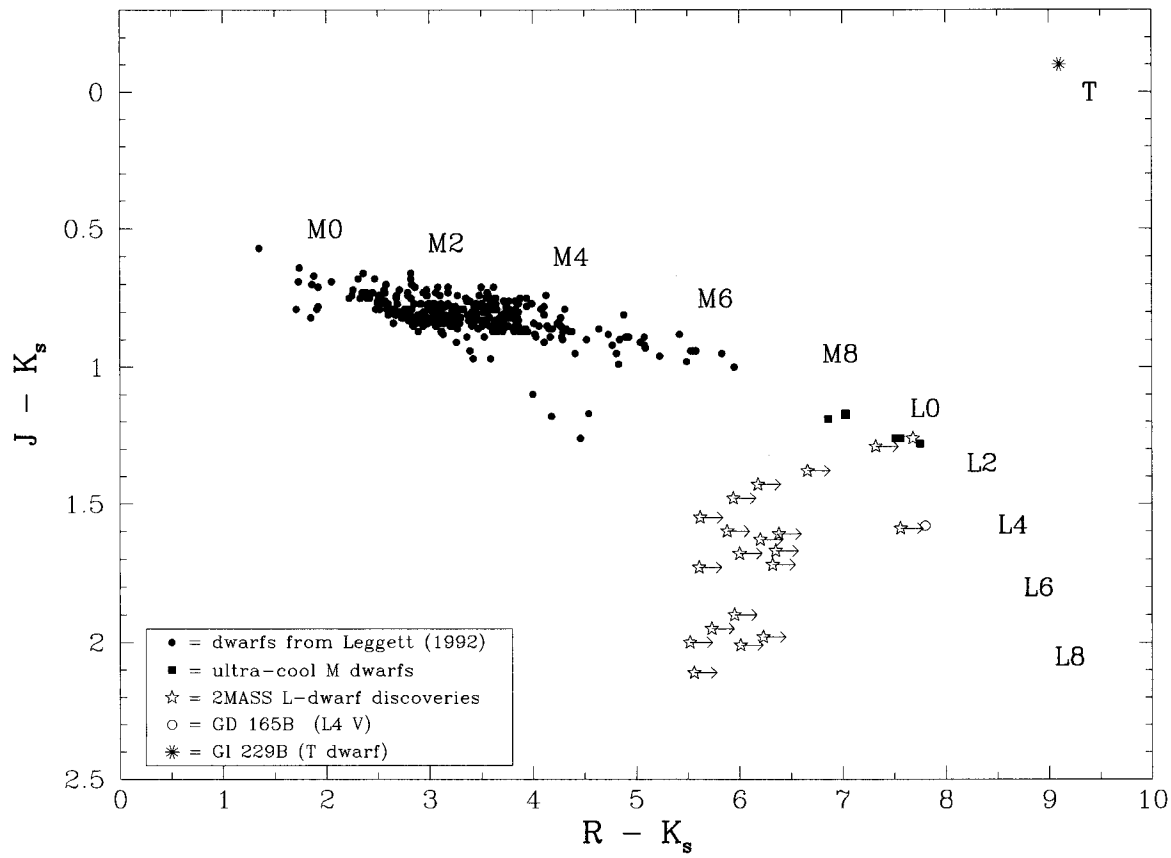

FIG. 1.—$J-K_s$ vs. $R-K_s$ diagram for cataloged M dwarfs (mostly from Leggett 1992), 2MASS discoveries from this paper, the brown dwarf candidate GD 165B, and the methane brown dwarf Gl 229B. Approximate spectral types (see § 5) are shown along the locus of points.

($J-K_s=-0.1$). (See Persson et al. 1998 for the definition of the K_s filter.) As Figure 1 shows, an optical minus infrared color is an excellent discriminant for brown dwarfs—their cool temperatures dictate faint optical magnitudes but much brighter near-infrared magnitudes—GD 165B has $R-K\approx 7.8$ and Gl 229B has $R-K_s=9.1$.

Using Figure 1 as a guide, we have searched for objects having $K_s\leq 14.50$ and no optical counterparts on the POSS-I R-band plate. The magnitude cutoff at K_s was chosen to ensure brighter objects with signal-to-noise ratios >10 since these could be more easily followed up spectroscopically and since the errors in the JHK_s magnitudes and colors would be smaller. We have selected against sources having optical counterparts on the red POSS-I plates to ensure colors of $R-K_s\geq 5.5$. From this list we have made a further cut by choosing only those objects with $J-K_s\geq 1.30$ (GD 165B–type analogs) or $J-K_s\leq 0.40$ (Gl 229B–type analogs) because the target list of objects having $0.40<J-K_s<1.30$ and $R-K_s\geq 5.5$ will be dominated by M dwarfs and asteroids.

In total 475 photometric scans acquired by the northern 2MASS facility between 1997 May and 1998 January were searched using the above criteria.[2] Each 2MASS scan covers an $8'.5\times 6^\circ$ region, and, taking into account overlaps between adjacent scans, our search covers 371 deg^2, or roughly 0.9% of the sky. Sixty-six objects meeting the above search criteria were found. Fifty-one objects with $J-K_s\geq 1.30$ are listed in Table 1A, and 15 objects with $J-K_s\leq 0.40$ are listed in Table 1B.[3] Tables 1A and 1B show the coordinate-based names[4] in column (1), Galactic latitude and longitude in columns (2) and (3) (or ecliptic latitude and longitude for objects in Table 1B), and the instrumental 2MASS-measured K_s magnitude and $J-K_s$ color in columns (4) and (5).

The objects in Table 1A were cross referenced via their coordinates against the SIMBAD database. The only one known previously is 2MASSs J0857258+172052, a high–Galactic-latitude extreme carbon star discovered in the *IRAS* Serendipitous Survey Catalog (Cutri et al. 1989). All of the objects in Table 1B, though having no optical counterparts and $J-K_s\leq 0.40$, were either identified by the 2MASS processing pipeline as known asteroids or flagged by hand as high proper-motion objects already tabulated in the Luyten Half-Second (LHS) Catalog

[2] An overview of the 2MASS project can be found in Skrutskie et al. (1997) and a discussion of the survey scanning strategy can be found in Kirkpatrick et al. (1997a).

[3] It should be noted that this search was conducted on output from an earlier version of the 2MASS processing pipeline that gave instrumental magnitudes only. For the purposes of this section, we will continue to refer to these instrumental magnitudes since they were the ones used for target selection, but in Tables 3 and beyond, we will refer to the final, calibrated magnitudes.

[4] Source designations for 2MASS discoveries are given as "2MASS*x* Jhhmmss[.]s±ddmmss." The "*x*" in the prefix will vary depending upon the catalog from which the object was taken; "P" is used for objects discovered in the prototype data, "SW" is used for objects taken from the actual survey's working database, and "Ss" is used for objects taken from the 2MASS Sampler release. The suffix conforms to IAU nomenclature convention and is the sexigesimal R.A. and decl. at J2000 equinox.

TABLE 1A

OBJECTS MEETING SEARCH CRITERIA IN 371 deg^2 (SUBSAMPLE WITH $J-K_s \geq 1.30$)

Object Name (1)	l (2)	b (3)	$(K_s)_{ins}$ (4)	$(J-K_s)_{ins}$ (5)	Observation Date (UT) (6)	Exposure (s) (7)	Spectral Type (8)
2MASSW J0010037+343610.....	111.3	−27.1	14.18	1.30	1997 Dec 09	1200	M8 V
2MASSW J0030438+313932.....	117.8	−31.0	13.82	1.43	1998 Jan 22	1200	(See Table 3)
2MASSW J0055384+275652.....	124.1	−34.9	14.20	1.39	1997 Dec 08	1200	M7 V
2MASSW J0129122+351758.....	131.6	−26.9	14.48	2.00	1998 Jan 23	3600	(See Table 3)
					1998 Jan 24	3600	
2MASSW J0147334+345311.....	135.8	−26.6	14.46	1.38	1997 Nov 09	2400	(See Table 3)
2MASSW J0149090+295613.....	137.6	−31.3	11.82	1.40	1997 Dec 07	2100	M9.5 V[a]
					1997 Dec 24	2400	
					1998 Jan 22	1200	
					1998 Jan 23	1200	
					1998 Jan 24	1200	
2MASSW J0242435+160739.....	158.2	−39.0	14.06	1.48	1998 Jan 24	2400	(See Table 3)
2MASSW J0245147+120350.....	161.8	−42.1	13.99	1.35	1997 Nov 09	900	M5 V
2MASSs J0251222+252124	154.4	−30.1	14.20	1.36	1998 Jan 23	1200	M9 V
2MASSs J0251253+262504	153.7	−29.2	14.30	1.40	1998 Jan 23	1200	M9 V
2MASSW J0326137+295015.....	158.7	−22.1	13.62	1.61	1998 Jan 24	1500	(See Table 3)
2MASSW J0326342+300012.....	158.7	−21.9	13.80	1.38	1998 Jan 24	300	Reddened bkg star[b]
2MASSW J0327091+300130.....	158.8	−21.8	14.35	2.41	1998 Jan 22	1200	Reddened bkg star[b]
2MASSW J0327205+294959.....	159.0	−21.9	13.82	1.85	1998 Jan 23	1200	Reddened bkg star[b]
2MASSW J0327210+295816.....	158.9	−21.8	14.12	1.38	1998 Jan 24	300	Reddened bkg star[b]
2MASSW J0327235+295230.....	158.9	−21.9	12.90	1.94	1998 Jan 22	1200	Reddened bkg star[b]
2MASSW J0327304+295558.....	158.9	−21.8	14.13	1.78	1998 Jan 24	300	Reddened bkg star[b]
2MASSW J0327364+294118.....	159.1	−22.0	13.98	1.31	1998 Jan 24	300	Reddened bkg star[b]
2MASSW J0328072+290424.....	159.6	−22.4	14.05	1.38	1998 Jan 24	300	Reddened bkg star[b]
2MASSW J0328543+293827.....	159.4	−21.9	14.40	1.43	1998 Jan 24	300	Reddened bkg star[b]
2MASSW J0329202+291734.....	159.7	−22.1	14.48	1.36	1998 Jan 24	300	Reddened bkg star[b]
2MASSW J0329214+290533.....	159.8	−22.2	13.79	1.49	1998 Jan 24	300	Reddened bkg star[b]
2MASSW J0329267+300057.....	159.2	−21.5	14.38	1.71	1998 Jan 24	300	Reddened bkg star[b]
2MASSW J0355419+225702.....	169.0	−23.0	14.05	1.91	1997 Dec 07	900	(See Table 3)
					1997 Dec 08	1200	
					1998 Jan 24	1200	
2MASSW J0401096+182808.....	173.5	−25.3	9.10	4.68	1997 Dec 08	600	Carbon star[c]
					1997 Dec 24	2400	
2MASSW J0724096+162302.....	201.7	14.5	14.40	1.31	1997 Dec 09	1200	M5.5 V
2MASSs J0850359+105716	216.5	31.4	14.27	1.94	1997 Nov 09	2400	(See Table 3)
					1997 Dec 07	1200	
					1997 Dec 08	1200	
					1997 Dec 09	1200	
					1998 Jan 24	4800	
2MASSs J0857258+172052	210.3	35.4	10.49	4.30	1998 Jan 22	1200	Carbon star[c,d]
2MASSW J0913032+184150.....	210.3	39.4	14.00	1.68	1998 Jan 22	2400	(See Table 3)
2MASSW J0914188+223813.....	205.6	40.9	13.68	1.38	1998 Jan 23	1200	M9.5 V
2MASSW J0918382+213406.....	207.3	41.6	13.68	1.72	1998 Jan 22	3600	(See Table 3)
2MASSW J0921457+191812.....	210.5	41.5	14.34	2.16	1998 Jan 22	2161	QSO[e]
2MASSW J1145572+231730.....	223.8	74.7	13.65	1.67	1997 Dec 07	1200	(See Table 3)
2MASSW J1146345+223053.....	226.8	74.6	12.44	1.59	1997 Dec 07	1200	(See Table 3)
2MASSW J1155009+230706.....	227.3	76.6	14.12	1.60	1998 Jan 22	2400	(See Table 3)
2MASSW J1159003+202056.....	239.6	76.2	14.47	1.39	1998 Jan 23	1200	M5.5 V
2MASSW J1214063+202702.....	249.0	79.2	14.18	1.30	1997 Dec 08	1200	M7 V
2MASSW J1239194+202952.....	279.6	82.8	12.99	1.38	1997 Dec 08	1200	M9 V
2MASSW J1314425+224103.....	354.1	83.1	14.47	1.75	1998 Jan 23	1200	M6 V
2MASSW J1320079+225722.....	1.8	82.3	14.36	1.51	1998 Jan 23	449	M6.5 V
2MASSW J1328550+211449.....	0.4	79.6	13.99	2.01	1997 Dec 08	2400	(See Table 3)
2MASSW J1334062+194034.....	357.9	77.7	13.80	1.64	1997 Dec 08	1200	(See Table 3)
2MASSW J1338333+292226.....	47.9	79.4	14.44	1.31	1998 Jan 23	1200	M6 V
2MASSW J1342236+175156.....	357.3	75.0	14.38	1.56	1997 Dec 09	1200	(See Table 3)
2MASSW J1434264+194050.....	20.9	65.3	14.09	1.31	1997 Dec 09	1200	M8 V
2MASSW J1439409+182637.....	19.4	63.7	14.39	1.73	1998 Jan 23	3600	(See Table 3)
					1998 Jan 24	2400	
2MASSW J1632291+190441.....	36.3	38.9	13.77	1.98	1998 Jan 23	3600	(See Table 3)
					1998 Jan 24	2400	
2MASSW J1710255+210715.....	42.3	31.2	14.19	1.55	1998 Jan 23	1200	M8 V
2MASSW J2258066+154416.....	86.9	−39.1	14.49	1.50	1997 Nov 08	2400	M7.5 V
2MASSW J2300189+121024.....	84.9	−42.3	14.19	1.34	1997 Nov 09	1200	M4.5 V

TABLE 1A—*Continued*

Object Name (1)	l(2)	b(3)	$(K_s)_{ins}$ (4)	$(J-K_s)_{ins}$ (5)	Observation Date (UT) (6)	Exposure (s) (7)	Spectral Type (8)
2MASSW J2308287+130928.....	87.9	−42.6	14.48	1.31	1997 Nov 09	900	M6 V

NOTE.—All spectroscopic observations were acquired with LRIS at the W. M. Keck Observatory except for the supplemental observations of 2MASSW J0149090+295613 and 2MASSW J0401096+182808 on 1997 December 24 (UT), which were acquired with DSpec at the Palomar 5 m telescope. See Liebert et al. 1999a, 1999b for details.

[a] See the companion paper by Liebert et al. 1999a.

[b] These are all reddened stars lying behind molecular clouds in Perseus.

[c] See the companion paper by Liebert et al. 1999b.

[d] This is the previously known carbon star IRAS SSC 08546+1732 (Cutri et al. 1989).

[e] See the companion paper by Cutri et al. 1999.

TABLE 1B

OBJECTS MEETING SEARCH CRITERIA IN 371 deg^2 (SUBSAMPLE WITH $J-K_s \leq 0.40$)

Object Name (1)	λ (2)	β (3)	$(K_s)_{ins}$ (4)	$(J-K_s)_{ins}$ (5)	Identification (6)	Observation Date (UT) (7)
2MASSW J0031007+332004.....	21.3	27.3	12.99	0.39	Asteroid (1235) Schorria	1997 Nov 15
2MASSs J0242258+294101	47.3	13.3	12.64	0.31	Asteroid 1981 YA1	1997 Nov 16
2MASSs J0244401+244224	46.3	8.4	13.06	0.38	Asteroid 1993 XO	1997 Nov 16
2MASSs J0251318+284917	49.0	11.8	13.37	0.35	Asteroid (3139) Shantou	1997 Nov 16
2MASSs J0251446+252347	48.0	8.6	12.45	0.27	Asteroid (1066) Lobelia	1997 Nov 16
2MASSs J0254141+275547	49.3	10.8	13.22	0.32	Asteroid (3300) McGlasson	1997 Nov 16
2MASSs J0849065+091520	132.1	−8.2	14.35	0.32	Asteroid (837) Schwarzschilda	1997 Nov 16
2MASSs J0850138+061125	133.2	−11.1	12.11	0.31	Asteroid (136) Austria	1997 Nov 16
2MASSs J0850274+073719	132.9	−9.7	9.04	0.39	Motion star LHS 2056	1997 Nov 16
2MASSW J0851360+174933.....	130.4	0.2	12.00	0.30	Asteroid (556) Phyllis	1997 Nov 15
2MASSW J0852144+161547.....	131.0	−1.3	14.35	0.28	Asteroid (2320) Blarney	1997 Nov 15
2MASSW J0915347+212728.....	134.8	5.3	13.57	0.38	Asteroid (2766) Leeuwenhoek	1998 Jan 12
2MASSW J0916286+231038.....	134.4	7.0	13.97	0.39	Asteroid (4041) Miyamotoyohko	1998 Jan 12
2MASSW J0924386+152849.....	138.6	0.3	11.93	0.39	Asteroid (569) Misa	1997 Nov 24
2MASSW J2251228+293944.....	357.4	33.8	13.73	0.31	Motion star LHS 529	1997 Nov 15

TABLE 2

OTHER OBJECTS OBSERVED AT KECK

Object Name (1)	l (2)	b (3)	$(K_s)_{ins}$ (4)	$(J-K_s)_{ins}$ (5)	Observation Date (UT) (6)	Exposure (s) (7)	Spectral Type (8)
A. Other 2MASS Discoveries							
2MASP J0147362+365855	135.2	−24.5	13.58	1.26	1997 Nov 09	1200	M7 V
2MASSW J0242252+134313.....	159.8	−41.1	13.25	1.21	1997 Nov 09	900	M6.5 V
2MASSW J0244087+171542.....	157.8	−37.9	14.47	1.26	1997 Nov 09	1200	M6.5 V
2MASSW J0244463+153531.....	159.1	−39.2	14.44	1.29	1997 Nov 09	1200	M5+M5.5 V
2MASP J0344232+253845	165.0	−22.8	13.43	1.51	1997 Nov 09	1200	M6.5 V
2MASP J0348036+234411	167.0	−23.6	12.98	1.43	1997 Nov 09	1200	M7.5 V
2MASSW J1439284+192915.....	21.6	64.1	11.35	1.26	1997 Dec 08	1200	(See Table 3)
2MASSW J1553214+210907.....	34.9	48.3	14.44	2.11	1998 Jan 23	1200	(See Table 3)
					1998 Jan 24	2400	
2MASSW J2041209−045943.....	41.4	−26.7	13.88	1.10	1997 Nov 09	1200	M5 V
2MASSW J2258379+162042.....	87.4	−38.6	13.69	1.20	1997 Nov 09	1200	M6 V
2MASSW J2258590+152047.....	86.8	−39.5	14.32	1.17	1997 Nov 09	900	M7 V
2MASSW J2305519+155404.....	89.1	−39.9	13.36	1.15	1997 Nov 09	900	M6 V
2MASSW J2309462+154905.....	90.1	−40.5	13.73	1.23	1997 Nov 08	1500	M8.5 V
B. Objects Observed as Comparisons							
2MASP J0345432+254023	165.2	−22.6	12.68	1.29	1997 Nov 09	1200	(See Table 3)
DENIS-P J0205.4−1159.....	175.5	−67.0	...	...	1997 Nov 09	1200	(See Table 3)
DENIS-P J1058.7−1548.....	267.1	39.1	...	...	1997 Dec 09	1200	(See Table 3)
DENIS-P J1228.2−1547.....	294.8	46.7	...	...	1997 Dec 09	1200	(See Table 3)
Kelu-1.....	307.0	37.1	...	...	1998 Jan 22	1200	(See Table 3)

TABLE 3

THE 25 L DWARFS AND GL 229B

Object Name (1)	Spectral Type (2)	K_s (3)	$J-K_s$ (4)	$H-K_s$ (5)	I_{spec} (6)	$I_{spec}-K_s$ (7)	Distance (pc) (8)
2MASP J0345432+254023	L0 V	12.70 ± 0.04	1.33 ± 0.05	0.53 ± 0.05	16.98	4.28	28.2*
2MASSW J0147334+345311.....	L0.5 V	13.59 ± 0.04	1.35 ± 0.06	0.57 ± 0.07	18.07	4.48	*32*
2MASSW J1439284+192915.....	L1 V	11.58 ± 0.04	1.18 ± 0.06	0.47 ± 0.06	16.02	4.44	15.1*
2MASSW J1439409+182637.....	L1 V	14.53 ± 0.11	1.68 ± 0.15	0.94 ± 0.17	19.87	5.34	*50*
2MASSW J1145572+231730.....	L1.5 V	13.87 ± 0.08	1.64 ± 0.10	0.57 ± 0.10	18.62	4.75	*35*
2MASSW J0242435+160739.....	L1.5 V	14.26 ± 0.08	1.41 ± 0.10	0.56 ± 0.10	19.01	4.75	*44*
2MASSW J1334062+194034.....	L1.5 V	13.99 ± 0.06	1.55 ± 0.09	0.84 ± 0.09	18.76	4.77	*38*
Kelu-1.....	L2 V	11.81 ± 0.03	1.57 ± 0.04	0.60 ± 0.04	16.51	4.70	*10**
2MASSW J0030438+313932.....	L2 V	13.99 ± 0.06	1.50 ± 0.08	0.59 ± 0.08	18.82	4.83	*35*
2MASSW J1342236+175156.....	L2.5 V	14.59 ± 0.11	1.47 ± 0.14	0.53 ± 0.13	19.81	5.22	*45*
2MASSW J0918382+213406.....	L2.5 V	14.21 ± 0.07	1.45 ± 0.10	0.43 ± 0.09	18.68	4.47	*30*
2MASSW J1146345+223053.....	L3 V	12.63 ± 0.04	1.60 ± 0.06	0.61 ± 0.08	17.62	4.99	*18**
DENIS-P J1058.7−1548.....	L3 V	12.53 ± 0.03	1.65 ± 0.04	0.69 ± 0.04	17.64	5.11	*23**
2MASSW J0913032+184150.....	L3 V	14.20 ± 0.05	1.72 ± 0.09	0.64 ± 0.08	19.07	4.87	*35*
2MASSW J0355419+225702.....	L3 V	14.25 ± 0.07	1.85 ± 0.11	0.78 ± 0.10	19.49	5.24	*35*
2MASSW J0326137+295015.....	L3.5 V	13.83 ± 0.06	1.60 ± 0.08	0.55 ± 0.08	19.17	5.34	*27*
2MASSW J0129122+351758.....	L4 V	14.68 ± 0.09	2.06 ± 0.18	0.61 ± 0.13	19.43	4.75	*39*
2MASSW J1155009+230706.....	L4 V	14.30 ± 0.12	1.68 ± 0.15	0.48 ± 0.15	19.30	5.00	*33*
GD 165B	L4 V	*14.15*	*1.58*	*0.65*	19.57	5.42	31.5
2MASSW J1328550+211449.....	L5 V	14.25 ± 0.10	1.79 ± 0.15	0.63 ± 0.13	20.07	5.82	*30**
DENIS-P J1228.2−1547.....	L5 V	12.81 ± 0.03	1.57 ± 0.05	0.56 ± 0.05	18.05	5.24	*17**
2MASSW J1553214+210907.....	L5.5 V	14.68 ± 0.12	2.00 ± 0.21	0.66 ± 0.19	20.79	6.11	*34*
2MASSs J0850359+105716	L6 V	14.46 ± 0.07	1.99 ± 0.14	0.76 ± 0.12	20.33	5.87	*41**
DENIS-P J0205.4−1159.....	L7 V	12.99 ± 0.04	1.56 ± 0.05	0.60 ± 0.05	18.28	5.29	16.6*
2MASSW J1632291+190441.....	L8 V	13.98 ± 0.05	1.88 ± 0.09	0.61 ± 0.07	19.98	6.00	*20**
Gl 229B	T dwarf	14.3	-0.1	0.0	19.53	5.23	5.8

NOTES.—The JHK_s photometry reported here is calibrated photometry, not instrumental values such as those listed in Tables 1A and 2. Please note that both the positional name and the calibrated photometry for the 2MASS objects may undergo slight revisions at a later date when the catalogs covering these scans are distributed to the community. Also note that the tabulated magnitude for GD 165B is K, not K_s. As explained in the text, photometry at the I-band (I_{spec}) is taken from the flux-calibrated Keck spectra. Italics in col. (8) indicate a distance estimated from the near-infrared magnitudes and the spectral type of the object; those not in italics are measured via trigonometric parallax. An asterisk (*) in this column indicates an object on the USNO parallax program.

(Luyten 1979a). Thus, all of our brown dwarf suspects with $J-K_s \leq 0.40$ were eliminated immediately, so none required spectroscopic follow-up. Identifications for these objects are given in column (6) of Table 1B along with the observation date (in col. [7]) of the 2MASS scan in which it was found. These objects will not be discussed further.

Several other objects not meeting the standard search criteria (not red enough to meet the $J-K_s \geq 1.30$ criterion or falling outside the 371 deg^2 search area) were also observed and are listed in the top portion of Table 2. Several late dwarfs selected from the literature and serving as comparisons were also observed. These are listed in the bottom portion of Table 2. The column descriptions are the same as in Table 1A.

3. FOLLOW-UP OBSERVATIONS

Targets in Table 1A and Table 2 were followed up using the Low Resolution Imaging Spectrograph (LRIS; Oke et al. 1995) at the 10 m W. M. Keck Observatory on Mauna Kea, Hawaii. A 400 line mm^{-1} grating blazed at 8500 Å was used with a 1″ slit and a 2048 × 2048 CCD to produce 9 Å resolution spectra covering the range 6300–10100 Å. Objects were observed during three separate observing runs on 1997 November 8 and 9 (UT), 1997 December 7, 8, and 9 (UT), and 1998 January 22, 23, and 24 (UT). Most of the run on 1997 November 8 (UT) was lost because of fog, but the other seven nights were photometric with generally excellent seeing (between 0.″6 and 0.″8 FWHM). Observation dates and exposure times for each target are given in columns (6) and (7) of Tables 1A and 2.

During the December and January runs, we used the OG570 order-blocking filter to eliminate second-order light. We erroneously used the GG495 filter during the November run, but because our targets are all extremely red with very little measurable flux below 6000 Å, the poor choice of filter affected only the much bluer flux calibration standards and only at wavelengths beyond 9900 Å. This effect was relatively easy to correct since we have the same flux standards taken with the correct OG570 filter in subsequent runs.

The data were reduced and calibrated using standard IRAF routines. A 1 s dark exposure was used to remove the bias, and quartz-lamp flat-field exposures were used to normalize the response of the detector. The individual stellar spectra were extracted using the APEXTRACT routine in IRAF, allowing for the slight curvature of a point-source spectrum viewed through the LRIS optics and using a template where necessary. Wavelength calibration was achieved using neon + argon arc lamp exposures taken after each program object. Finally, the spectra were flux calibrated using observations of standards LTT 9491, Hiltner 600, and LTT 1020 from Hamuy et al. (1994). The data have not been corrected for telluric absorption, so the atmospheric O_2

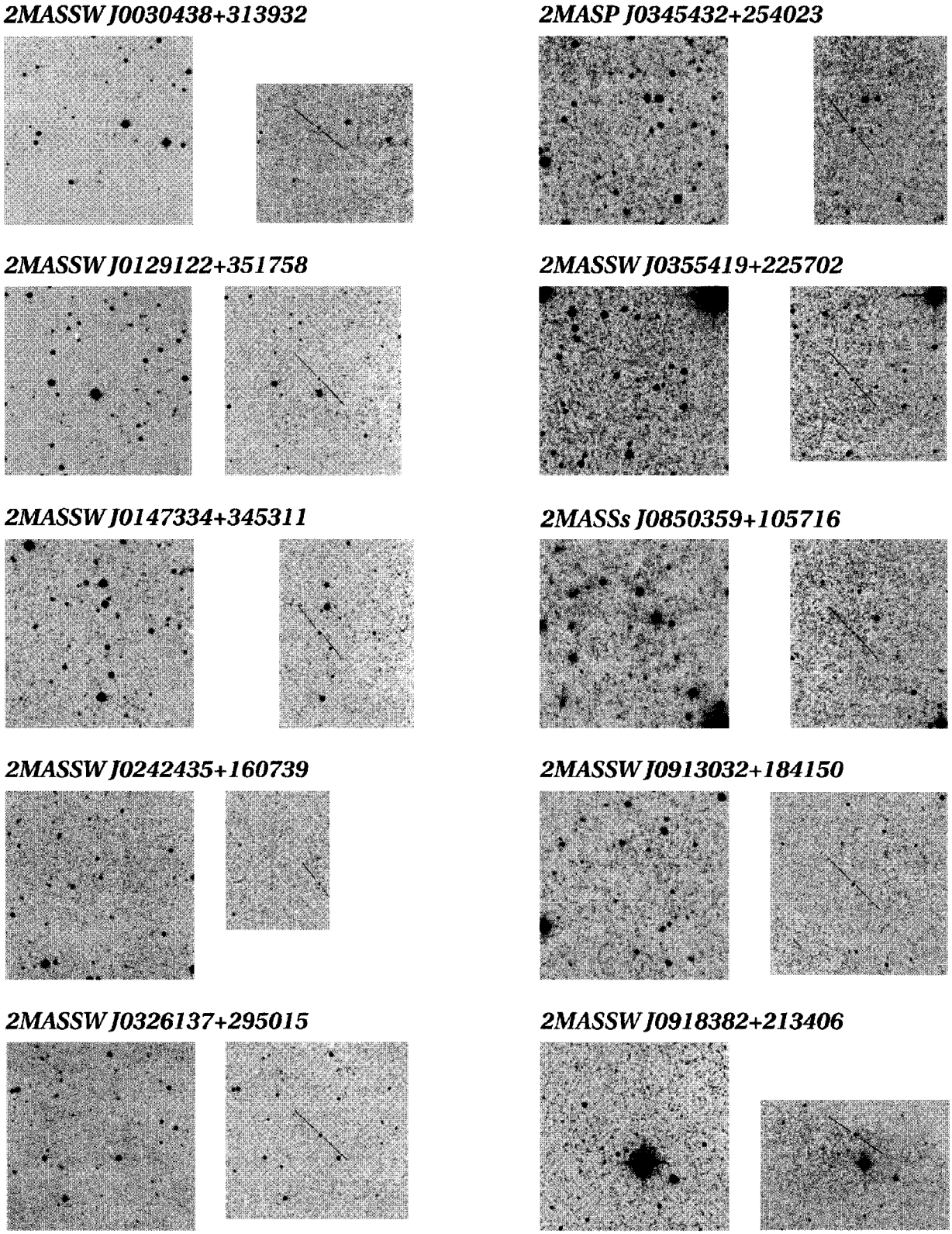

FIG. 2.—Finder charts for each of the 2MASS L dwarfs listed in Table 3. For each object, two views are shown—the POSS-I E (R-band) image on the left and the 2MASS K_s-band image on the right. Each view is to the same scale, 5′ on a side with north up and east to the left. The L dwarf is labeled with tick marks on the 2MASS image. Note that the POSS-I image is centered on the position of the 2MASS object and that the 2MASS image does not always cover the full 5′ × 5′ field.

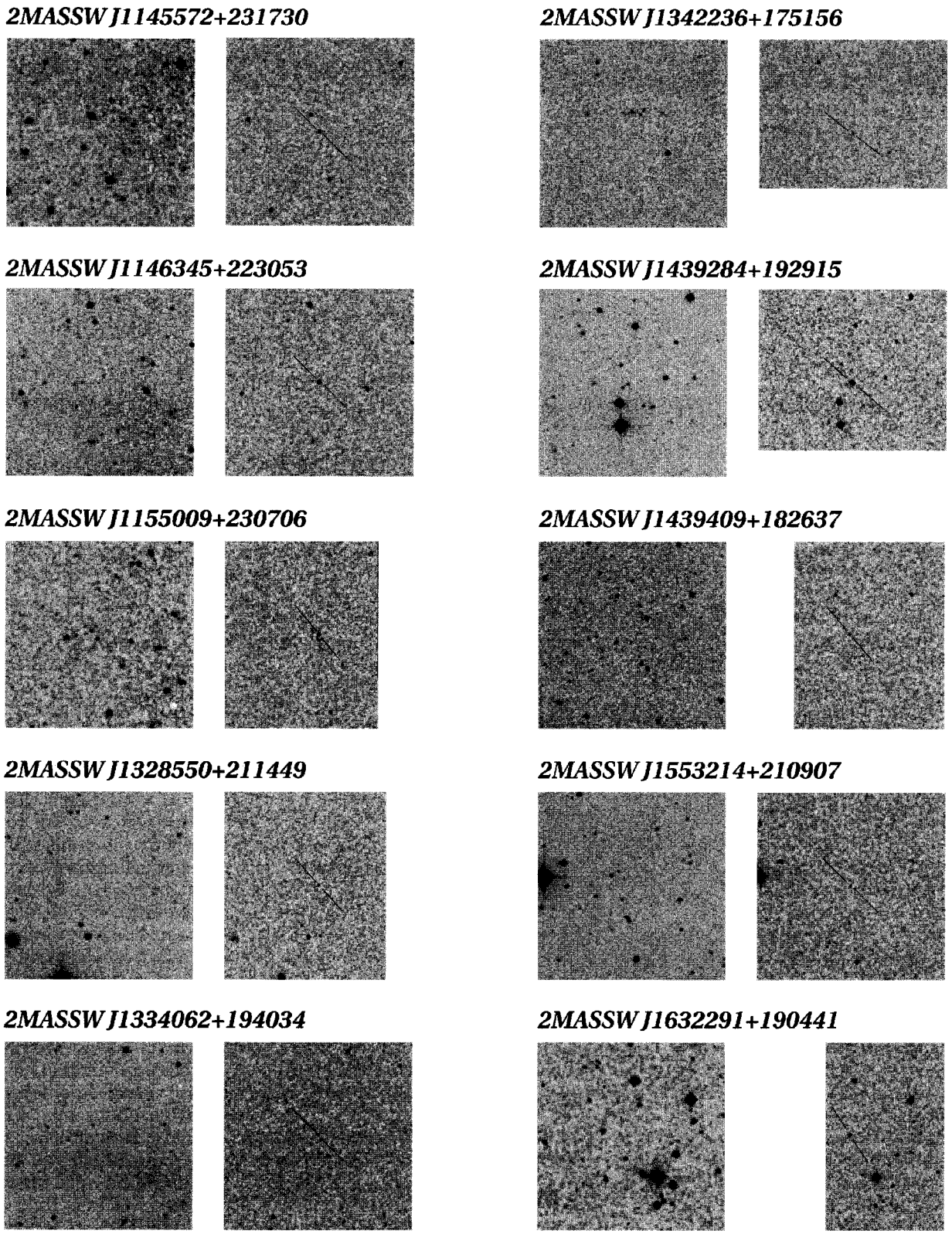

FIG. 2.—*Continued*

bands at 6867–7000, 7594–7685 Å and H_2O bands at 7186–7273, 8161–8282, ~8950–9300, ~9300–9650 Å are still present in the spectra.

Classifications based on the resulting spectra are given in column (8) of Tables 1A and 2. With one exception, all of the objects between R.A. = 03^h26^m and 03^h30^m are background stars heavily reddened by intervening molecular clouds in Perseus. For M dwarfs, spectral types were assigned using the least-squares minimization technique described in Kirkpatrick, Henry, & McCarthy (1991) using spectral standards previously observed at similar resolutions and over the same wavelengths as those described here. For M

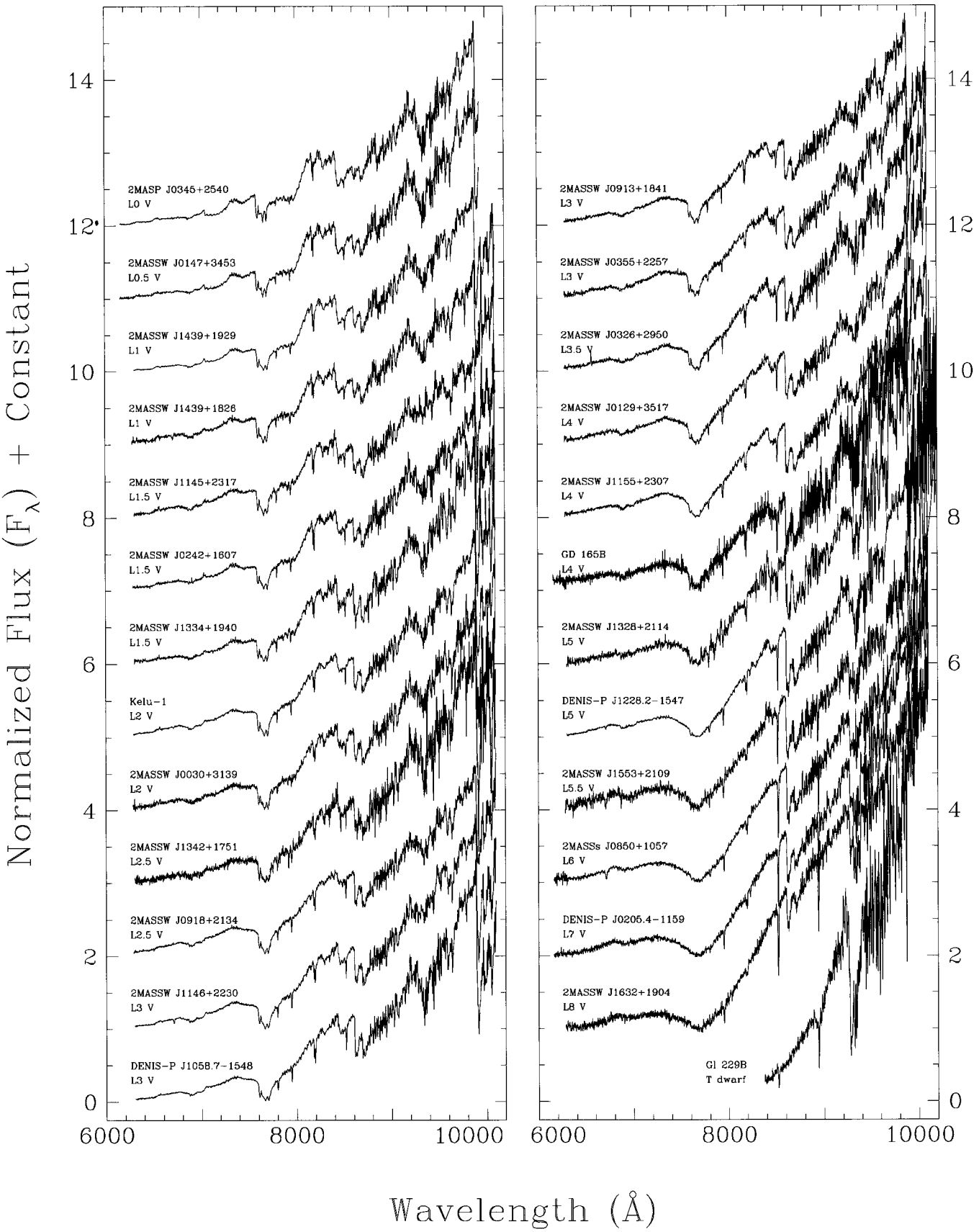

FIG. 3.—Spectra of all 26 dwarfs listed in Table 3. The flux scale is in units of F_λ normalized to one at 8250 Å. Integral offsets have been added to the flux scale to separate the spectra vertically. All spectra shown here were taken during our Keck follow-up runs except for the spectrum of GD 165B, which is from Kirkpatrick et al. (1999), and that of Gl 229B, which is from Oppenheimer et al. (1998). Names for the 2MASS objects have been abbreviated.

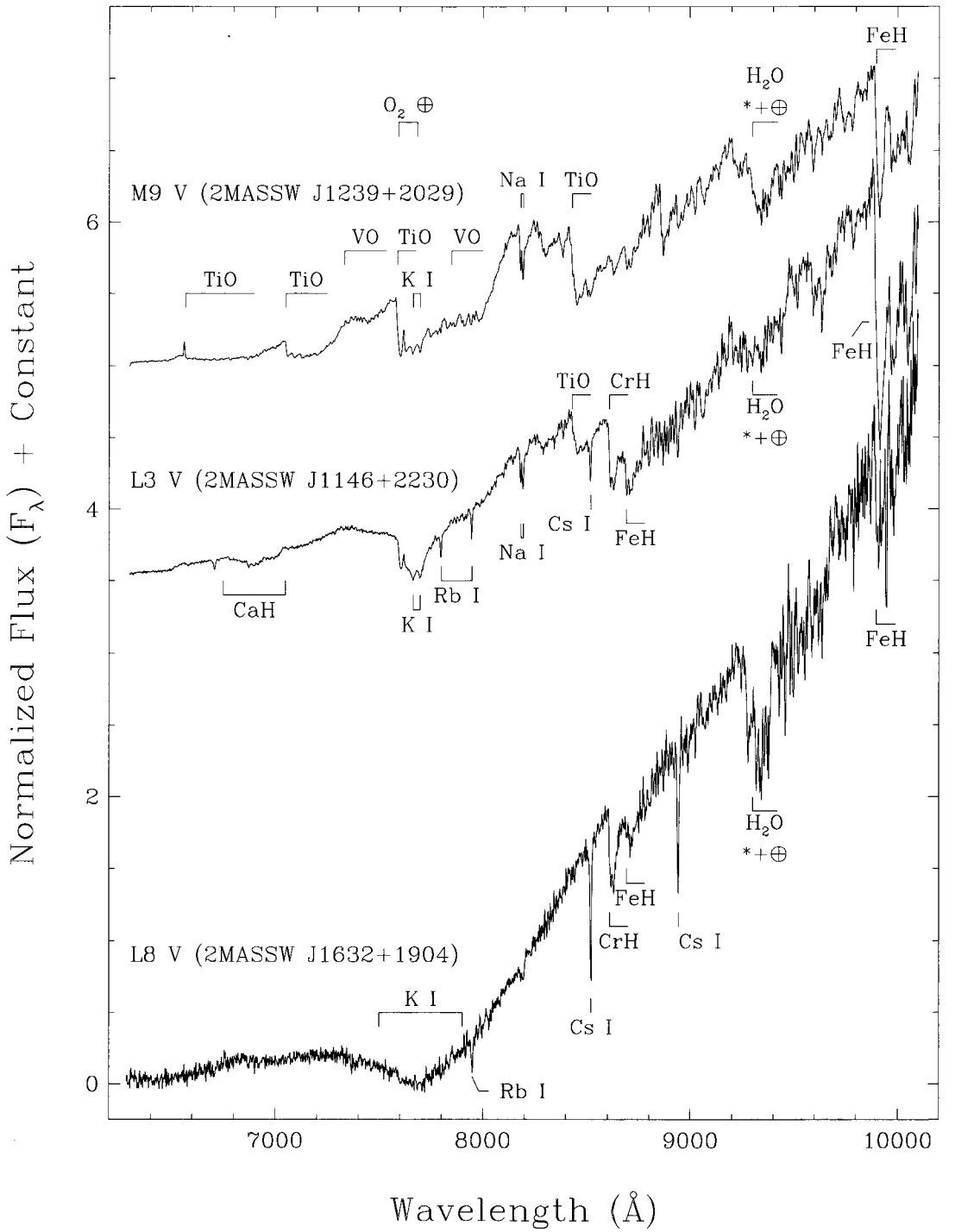

FIG. 4.—Enlarged spectra of a late-M, early- to mid-L, and late-L dwarf. Prominent features are marked. Note the absence of oxide absorption in the L dwarfs along with the dominance of alkali lines and hydride bands. Names for the 2MASS objects have been abbreviated.

dwarfs of type M7 and later, these types were refined using the VO ratio described in Kirkpatrick, Henry, & Irwin (1997b).

All dwarfs later than spectral type M9.5 are discussed in the next section, and notes on individual M9.5+ dwarfs can be found in Appendix A. Notes on other interesting objects can be found in Appendix B.

4. RESULTS FOR DWARFS COOLER THAN TYPE M9.5 V

Listed in Table 3 are all the dwarfs from Tables 1A and 2 that have spectral types cooler than M9.5 V. This includes the 2MASS dwarf discovered in Prototype Camera data (Kirkpatrick et al. 1997a), Kelu-1 discovered during the course of the proper-motion survey of Ruiz, Leggett, & Allard (1997), and the three cool dwarfs discovered by the Deep Near Infrared Survey (DENIS; Delfosse et al. 1997; Tinney, Delfosse, & Forveille 1997). Also included in the table for comparison purposes are the only two companion objects currently known with spectral types cooler than M9.5 V: GD 165B and Gl 229B. In total, 26 dwarfs have been found with post-M9.5 types, and 20 of those are from 2MASS. Optical and near-infrared finder charts for the

TABLE 4

L-DWARF FEATURE IDENTIFICATIONS IN THE FAR-OPTICAL

Atom/ Molecule (1)	Location (Å) (2)	Transition (3)
Hα[a]	6563	$3d\ ^2D_{5/2}-2p\ ^2P_{3/2}$
Li I[a].....	6708	$2s\ ^2S_{1/2}-2p\ ^2P_{3/2,1/2}$
CaH[a,b]...	Broad trough ~6750–7050	0–0 band of $A\ ^2\Pi-X\ ^2\Sigma$
TiO[a]	7053 head, degraded to red	0–0 band of $A\ ^3\Phi-X\ ^3\Delta$
VO[a].....	Broad trough ~7334–7534	1–0 band of $B\ ^4\Pi-X\ ^4\Sigma^-$
TiO[a]	7589 head, degraded to red	0–1 band of $A\ ^3\Phi-X\ ^3\Delta$
K I[b].....	7665	$4s\ ^2S_{1/2}-4p\ ^2P_{3/2}$
K I.....	7699	$4s\ ^2S_{1/2}-4p\ ^2P_{1/2}$
Rb I.....	7800	$5s\ ^2S_{1/2}-5p\ ^2P_{3/2}$
VO[a].....	Broad trough ~7851–7973	0–0 band of $B\ ^4\Pi-X\ ^4\Sigma^-$
Rb I.....	7948	$5s\ ^2S_{1/2}-5p\ ^2P_{1/2}$
Na I	8183	$3p\ ^2P_{1/2}-3d\ ^2D_{3/2}$
Na I	8195	$3p\ ^2P_{3/2}-3d\ ^2D_{5/2,3/2}$
TiO[a]	8206 head, degraded to red	0–2 band of $A\ ^3\Phi-X\ ^3\Delta$
TiO[a]	8432 head, degraded to red	0–0 band of $E\ ^3\Pi-X\ ^3\Delta$
Cs I.....	8521	$6s\ ^2S_{1/2}-6p\ ^2P_{3/2}$
CrH	8611 head, degraded to red	0–0 band of $A\ ^6\Sigma^+-X\ ^6\Sigma^+$
FeH	8692 head, degraded to red	1–0 band of $A\ ^4\Delta-X\ ^4\Delta$
Cs I.....	8943	$6s\ ^2S_{1/2}-6p\ ^2P_{1/2}$
H_2O[b] ...	Broad trough around ~9300	$\nu_1+\nu_3=3$
VO[a,b]....	Broad trough ~9540–9630	1–0 band of $A\ ^4\Pi-X\ ^4\Sigma^-$
FeH	9896 head, degraded to red	0–0 band of $A\ ^4\Delta-X\ ^4\Delta$
CrH	9969 head, degraded to red	0–1 band of $A\ ^6\Sigma^+-X\ ^6\Sigma^+$

[a] Feature not seen in all L dwarfs.
[b] Contaminated by telluric absorption bands.

2MASS objects are shown in Figure 2.

Spectra for each of the objects in Table 3 are shown in Figure 3. These are ordered in temperature from the warmest at top left to the coolest at bottom right. Two of these spectra are shown in detail in Figure 4 along with the spectrum of a late-M dwarf for comparison.

Immediately apparent in this spectral sequence is the quick disappearance of TiO bands, the hallmark of spectral type M. In fact, metallic oxides (TiO and VO) are replaced by metallic hydrides—CrH at 8611 and 9969 Å and FeH at 8692 and 9896 Å—as the major molecular species in these objects. Also strong are neutral atomic lines of alkali metals: Na I (8183, 8195 Å), K I (7665, 7699 Å), Rb I (7800, 7948 Å), Cs I (8521, 8943 Å), and sometimes Li I (6708 Å). A comprehensive list of features is given in Table 4.

Because these objects are so fundamentally different spectroscopically from M dwarfs, we feel that a new spectral class beyond "M" is warranted. The choice of new letter, along with the definition of each of the new subclasses, is discussed in the next section.

5. DEFINING THE NEW SPECTRAL CLASS

5.1. *Choosing the Letter*

In choosing a letter designation for the new spectral class, three important points must be considered: (1) The letter must be unambiguous, having not been used for any currently recognized spectral type. For example, though "N" follows "M" in the alphabet, it would be a poor choice of letter since it is used for a class of carbon stars. (2) The letter must create a taxonomy that is clearly distinguished from other types of astronomical objects. In this case, the letter must be accepted by the entire community, both by researchers involved in low-mass star and brown dwarf science and by astronomers in general. Although stellar spectroscopists might find "E0," "E1," "E2," etc., perfectly acceptable as new spectral subclasses, extragalactic morphologists already recognize these designations as elliptical galaxy types. (3) The letter must stand the test of time. For example, choosing "D" to mean that these objects are "degenerate" brown dwarfs would be flawed reasoning. Some of these dwarfs certainly are substellar (see § 7), but such a designation cannot be tied uniquely to any particular spectroscopic trait. The designation should apply to spectral features alone and be free of physical interpretation. Our understanding of the underlying physics may change with time; our choice of letter should be impervious to such changes.

In considering point 1, we should briefly examine the history of stellar spectral classification. One of the earliest attempts at classification was provided by Secchi (1866) who grouped stellar spectra into four classes called I, II, III, and IV. Later, the Henry Draper Memorial Catalogue (Pickering 1890) provided classifications for over 10,000 stars based on the Secchi types as further subdivided and renamed by Williamina Fleming. This system used ABCD to subdivide Secchi's type I, EFGHIKL to subdivide Secchi's type II, M for Secchi's type III, N for Secchi's type IV, O for Wolf-Rayet stars, P for planetary nebulae, and Q for unclassified objects. Thus, the Fleming system used all letters except for J and for R through Z. It was a few years later when Annie Jump Cannon dropped the redundant letters and reordered the remaining ones into the OBAFGKM sequence used today (Cannon & Pickering 1901).

Except for OBAFGKM, the only other letter retained from the Fleming system was N, used to designate the carbon stars first recognized by Secchi. Later, Pickering (1908) announced the discovery of a new class of carbon star, which he denoted R, acknowledging that letters up through Q had been used previously. Several years later, class S was introduced (Cannon & Pickering 1923) for stars with prominent ZrO bands. The letter J, skipped in the Fleming classification system, was used to denote a subset of the R and N stars having strong ^{13}C features (Bouigue 1954; Gordon 1971). Meanwhile, Keenan & Morgan (1941) invented a new scheme for classifying carbon stars and used the letter C—the first letter to be recycled from the Fleming system.

Since there is a precedent for reusing the Fleming letters, this means that D, E, H, I, L, P, Q, and T–Z are still available as new designations. Table 5 lists the letters of the alphabet, identifying which ones are currently in use and which of those remaining should be avoided once we consider points 2 and 3.

The results of Table 5 show that the best remaining letters are H, L, T, and Y. (See also Kirkpatrick 1998.) We discuss the pros and cons of each letter below.

"L."—This seems to be the best choice simply because it is the remaining letter that is alphabetically closest to "M." This letter, recycled from the Fleming system, is not currently used for any spectral class.

"H."—This letter might be a better choice because, unlike "L," "H" could carry some meaning—it could indicate that these dwarfs are dominated by *h*ydrides. However, none of the main-sequence types OBAFGKM carry any meaning, and the term "hydride dwarf" is used occasionally to refer to M subdwarfs dominated by CaH

TABLE 5

SUMMARY OF LETTERS TO GUIDE CHOICE OF NEW SPECTRAL TYPE

Letter (1)	Status (2)	Notes (3)
A	In use	Standard spectral class
B	In use	Standard spectral class
C	In use	Standard carbon-star class
D	Ambiguous	Confusion with white dwarf classes DA, DB, DC, etc.
E	Ambiguous	Confusion with elliptical galaxy morphological types E0–E7
F	In use	Standard spectral class
G	In use	Standard spectral class
H	OK	
I	Problematic	Transcription problems with I0 (10, Io) and I1 (11, II, Il)
J	In use	Standard carbon-star class
K	In use	Standard spectral class
L	OK	
M.....	In use	Standard spectral class
N	In use	Standard carbon-star class
O	In use	Standard spectral class
P	Problematic?	Incorrect association with planets?
Q	Problematic?	Incorrect association with QSOs?
R	In use	Standard carbon-star class
S.....	In use	Standard spectral class for ZrO-rich stars
T	OK	
U	Problematic?	Incorrect association with ultraviolet sources?
V	Problematic	Confusion with vanadium oxide (V0 vs. VO)
W.....	Ambiguous	Confusion with Wolf-Rayet WN and WR classes
X	Problematic	Incorrect association with X-ray sources
Y	OK	
Z	Problematic?	Incorrect implication that we have reached "the end"?

and MgH bands. Like "L," "H" is not currently in use and would be a recycling of a previous Fleming class.

"T" *or* "Y."—If we take the position of purists and say that letters should not be recycled, then this leaves only "T" and "Y." This stance, however, leaves very little room for extending the sequence further. We already know of one cooler object (Gl 229B) that does not fit into the new spectral sequence because it is so much colder than the others. Its spectrum is dominated by methane, much like the Jovian planets. Hence, once we have enough objects similar to Gl 229B, they too will require a new letter since they are fundamentally different from the dwarfs discussed here.

Because "L" has a slight edge over "H" and both are preferred to "T" or "Y," we will adopt "L" as the designation for the new class of objects.[5] For cooler spectra, we will attempt to go in alphabetical order from "L," thus making "T" the class for the methane-dominated spectra of the Gl 229B type.

We must reemphasize, however, that "L" does not carry any meaning—these objects should not be referred to as *l*ithium dwarfs since at least two-thirds show no lithium at low resolution (see § 7) or *l*ow-luminosity dwarfs since Gl 229B (a non-L) is lower in luminosity. Because some of these objects are substellar and thus not truly stars, the entire collection should be referred to as "L dwarfs," not "L stars." This will also eliminate any confusion with L* galaxies. So that these new spectral types are more recognizable *as* spectral types, we will append a luminosity class V on them even though L-class objects do not exist for other luminosity classes such as III or I.

As another consideration on choice of letter, it should be noted that as the giant sequence has been pushed to cooler temperatures, M types have been retained. Giant classes M10 and M11 are sometimes seen in the literature (Bessell 1991). These objects are still dominated by strong bands of TiO and VO, so it is reasonable to continue the M sequence to higher numbers. Some critics have argued that the latest M types break with the tradition of the standard Morgan, Keenan, & Kellman (1943) system, which stipulates that objects of the same spectral class but different luminosity classes have essentially identical temperatures. Bessell (1991), in attempting to force this requirement on the classification of the latest M dwarfs, advocates a system that collapses the Boeshaar & Tyson (1985) types M7 through M9 into a single subclass.

However, the difference in luminosity between late-M dwarfs and giants exceeds five orders of magnitude and the surface gravities also differ by five orders of magnitude. Thus, the physical processes that dominate dwarf and giant spectra will be clearly dissimilar. Forcing the late-M dwarfs to follow the same mapping of temperature into spectral type as the late-M giants is unnecessary. Besides, dwarfs of classes M7, M8, and M9 have distinct taxonomic differences and should not be relegated to a single subtype. Therefore we will retain the late-M dwarf classification of Boeshaar & Tyson as further refined by Kirkpatrick et al.

[5] Martín et al. (1997) have also noted that "L" would be a good choice of letter. We disagree, however, with their suggestion that the L class be divided into L_{Li} and L_{CH_4} categories since the onset of methane—because it changes the near-infrared spectrum of Gl 229B so dramatically from the L dwarfs (Fig. 5)—justifies a new class in its own right. The emphasis of Martín et al. seems to be in distinguishing brown dwarfs from stars, and this is further reflected in their suggestion to create new M classes with designations such as "bdM_{Li}." The problem here is that the lithium line is often very weak, so in order to assign a class accurately we would need both low-resolution spectra to assign temperature subclasses 0, 1, 2, etc., and high-resolution spectra to assign the Li subscript. Furthermore and more importantly, not all brown dwarfs have lithium and not all M dwarfs with lithium are substellar. For these objects, creating a taxonomy that mixes spectral features with our (current) understanding of the physics should, as stated earlier, be avoided.

(1991, 1997b) and use those as a starting point for the L-dwarf sequence.

5.2. *Defining the Subclasses*

5.2.1. *Considerations*

In defining the individual subclasses, there are two questions that need to be addressed. (1) Over what wavelength range and at what resolution will the L-dwarf and T-dwarf classification systems be defined? (2) Do the coolest of the 2MASS and DENIS discoveries show methane, thus demonstrating a passage from L-type to T-type? If not, what should the subclass of these coolest known L dwarfs be in order to have a sufficient number of future subclasses for even cooler L dwarfs?

In answer to question 1, we have chosen a spectral region and resolution very similar to those used in Kirkpatrick et al. (1991) to define M-dwarf classes. Namely, for the L dwarfs, we choose the far-optical spectral region[6] between 6500 and 10,000 Å at a resolution of 9 Å. As shown by the listing of Table 4, this spectral region includes several bands of TiO and VO that can be used to differentiate between the latest M dwarfs and the earliest L dwarfs. The region also includes one set each of resonance lines from the neutral alkali metals Li, Na, K, Rb, and Cs as well as two bands each of CrH and FeH—many of which can be used to judge temperature.

Use of this spectral region gives access to many spectral diagnostics, but the drawback is that L dwarfs are exceedingly faint at these wavelengths. Thus, a very large aperture telescope is required to observe the spectra. A solution would be to use the near-infrared (1–2.5 μm) spectrum, in which the flux is greatly enhanced relative to the optical. We know from the spectra of late-type M dwarfs (Kirkpatrick 1994) that the H and K bands are largely devoid of spectral diagnostics, but at the J-band there are two sets of K I doublets along with FeH bands, which can serve as temperature discriminants. It should therefore be possible to set up L-dwarf classification criteria based on J-band spectra alone.

As for T dwarfs—which we will define as dwarfs exhibiting methane absorption at the K-band—Oppenheimer et al. (1998) have shown that Gl 229B has few distinguishable features in the far-optical—the two Cs I lines, a weak CH_4 band near 8900 Å, and an H_2O band around 9300 Å. Moreover, even Gl 229B, at a distance of only 5.8 pc, is exceedingly dim at these wavelengths ($R \approx 23.4$ and $I \approx 19.5$; Golimowski et al. 1998). Thus, for the T dwarfs we will be forced to rely on near-infrared spectra. Fortunately, the distinguishing feature of T-class objects—methane—has very prominent bands in both the H and K spectral regions. Once we have identified objects that span the very late-L and early-T range, we will establish criteria in both the far-optical and near-infrared that can be used to distinguish class L from class T.

5.2.2. *Additional Observations*

This leads to question 2: have we already identified objects crossing the late-L/early-T border? Delfosse et al. (1997) claimed a possible detection of methane in the K-band spectrum of their coolest discovery, DENIS-P J0205.4−1158. To check for methane in the 2MASS dwarfs, we applied for service time on the United Kingdom Infrared Telescope (UKIRT) to acquire K-band spectra of our two coolest objects, 2MASSs J0850359+105716 and 2MASSW J1632291+190441, which bracket DENIS-P J0205.4−1158 in temperature (see Fig. 3).

Observations were carried out on 1998 February 18 (UT) using the Cooled Grating Spectrometer 4 (CGS4) equipped with a 40 line mm^{-1} grating and 0.″6 slit. The grating was used in first order with a central wavelength of 2.21 μm to cover the range 1.89–2.53 μm. The resulting resolution is $R = 880$. The targets were nodded along the slit and observations taken in ABBA sequences. At each of the four nod positions, four 30 s exposures were acquired with half-pixel stepping between each to provide optimum sampling. Many such sequences were taken. The total exposure time for 2MASSs J0850359+105716 was 72 minutes, and for 2MASSW J1632291+190441 it was 64 minutes. Bracketing the observations of the targets, early-A type stars at similar air masses were also observed to facilitate corrections for telluric absorption and to serve for flux calibration. Argon arcs were taken for wavelength calibration.

In addition, 2MASSW J1632291+190441 was also observed on 1998 February 20 (UT) to acquire the entire water band between H and K. The same setup as above was used except that the central wavelength was set to 1.98 μm to cover the range 1.67–2.31 μm. In this case, a xenon arc was used for wavelength calibration.

For both sets of observations, data were reduced as follows. Under the UKIRT service time program, the data were already bad-pixel masked, flat fielded, sky subtracted, and co-added into a single ABBA image. Spectra were then extracted using the APEXTRACT package of IRAF. Spectra and their corresponding arcs were extracted using identical traces along the array. The extractions were then wavelength calibrated and corrected for telluric absorption by dividing by the A-type spectral standard taken at a similar air mass.[7] Flux calibration was obtained by assuming the A-type standards are blackbodies at the temperatures inferred from their published spectral types. Finally, the individual ABBA spectra were summed into one final spectrum for each target, and the flux scaling of this final spectrum normalized to one at 2.20 μm.

The resulting spectra are shown in Figure 5. For comparison, the Gl 229B spectrum of Geballe et al. (1996)—also acquired with CGS4 on UKIRT—is shown as well. Both of the 2MASS spectra show CO band heads and no trace of CH_4. Thus, we believe that the feature seen in the Delfosse et al. spectrum of DENIS-P J0205.4−1158 is not attributable to methane either, since that object's optical spectrum shows that it is intermediate in temperature between the two 2MASS objects displayed in Figure 5.

5.2.3. *Establishing the Grid of Subclasses*

The conclusion from Figure 5, then, is that we have yet to detect the onset of methane absorption at 2.2 μm in the 2MASS discoveries. This is consistent with the fact that the

[6] If instrumental restrictions prohibit the acquisition of spectra identical to this, a smaller wavelength coverage at identical resolution will suffice. In this case, coverage between 7000 and 9000 Å is adequate for classification purposes.

[7] There are residuals in the final spectra due to 1.817 μm Brϵ, 1.875 μm Pα, and 1.944 μm Brδ absorptions in the A-type star because these could not be disentangled from the deep telluric absorption between 1.80 and 1.95 μm. Other stellar absorptions in the A-type star were removed before division.

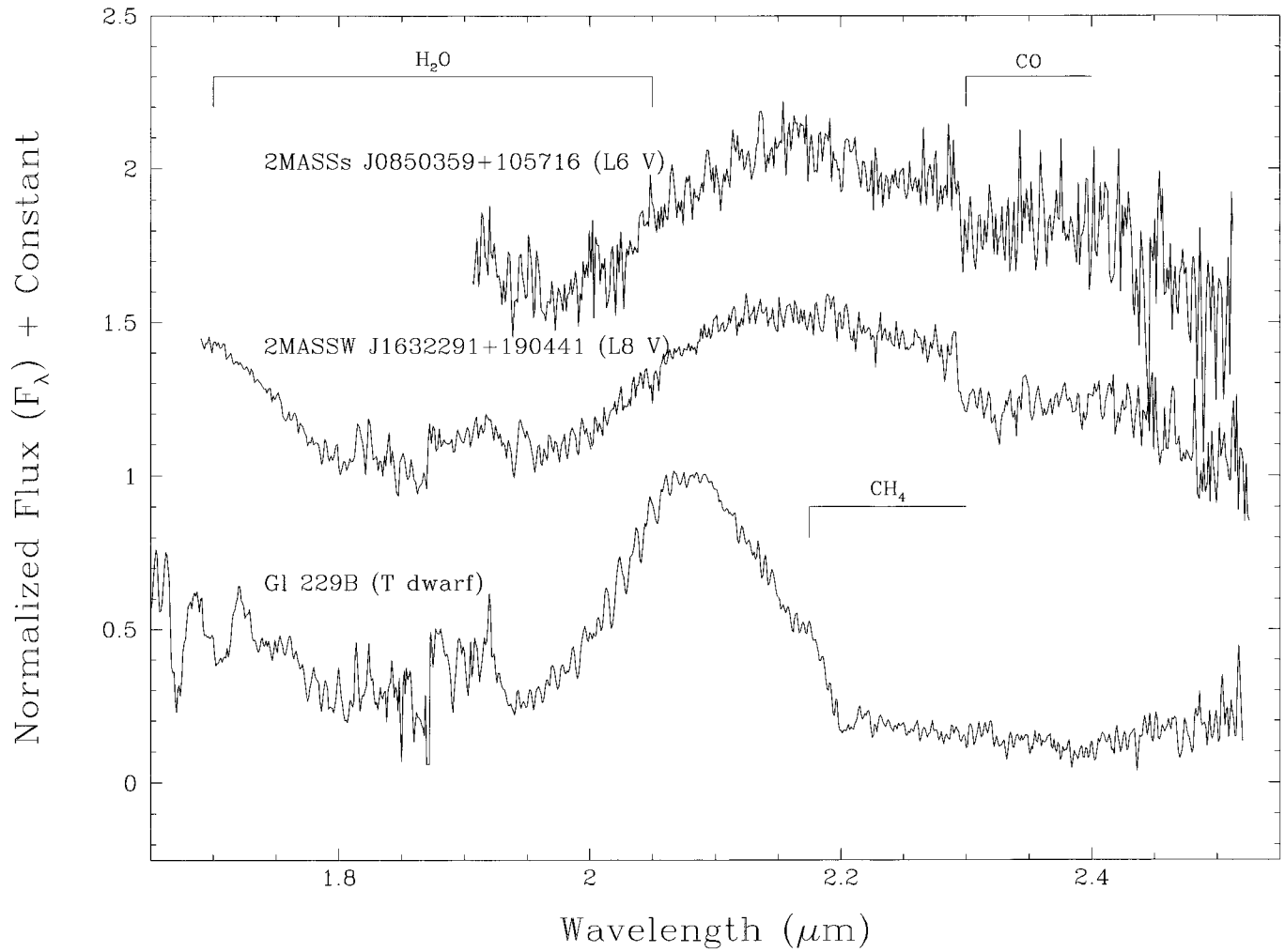

FIG. 5.—Near-infrared spectra of the two coolest 2MASS L dwarfs, taken with CGS4 on UKIRT. Also shown for comparison is the Geballe et al. (1996) spectrum of the only known T dwarf Gl 229B, also taken with CGS4 on UKIRT. The flux scale is in units of F_λ normalized to one at 2.20 μm. Integral offsets have been added to the flux scale to separate the spectra vertically. Note the absence of methane absorption and the continued presence of CO absorption in the late-L dwarfs.

2MASS $J-K_s$ colors are, with some cosmic scatter, increasing with cooler types. (Refer to § 6.1 and Fig. 13 for more on this.) Once methane has appeared at the K_s-band, we would expect the $J-K_s$ color to turn bluer, as it does in Gl 229B.

It should be noted here that the search for infrared-selected QSOs (Cutri et al. 1999) has identified candidates over a larger area of sky than that surveyed here ($\sim$1900 deg^2, or roughly 5 times as much coverage as our survey), and only seven additional IR-only sources with $J-K_s >$ 2.00 beyond those listed in Tables 2 and 3 were found. All of these have been observed spectroscopically, and none of the confirmed L dwarfs are cooler than the coolest shown in this paper. Because of the much larger area of the QSO search and its lack of success in uncovering redder L dwarfs, we believe that we already have objects near the breakpoint between classes L and T. In other words, objects with temperatures cooler than 2MASSW J1632291+190441 will have $J-K_s$ colors less than $\sim$2.00 or perhaps considerably less than $\sim$2.00 depending upon how quickly the onset of methane absorption occurs with temperature. However, to leave room for additional L types in case cooler non-methane objects are discovered, we will set the spectral type of 2MASSW J1632291+190441 to be L8 V.

Table 6 establishes qualitative spectral diagnostics that define each subclass from L0 through L8. Also listed in the table is a bright representative object for each subclass. These objects can be regarded as the primary spectral standards. Figure 6, a subset of Figure 3, serves as a visual guide to Table 6 by showing these primary standards in greater detail and comparing them to spectra of late-M dwarfs and the only known T dwarf. Figure 7 shows blow-ups of the spectra from 7300–8000 Å and 8400–9000 Å to help further illustrate the criteria of Table 6.[8]

As one final note about defining the latest L subclasses, it is reasonable to imagine, after looking at Figures 6 and 7, that an L9 dwarf would have imperceptible FeH bands and much weaker CrH bands than the L8 dwarf 2MASSW J1632291+190441. Once these hydrides have disappeared from the far-optical spectra, the result will be an almost smooth spectrum much like that of the methane brown

[8] It should be noted that a few late dwarfs previously assigned "$\geq$M" and later designations in Kirkpatrick, Henry, & Simons (1995) and Kirkpatrick et al. (1997b) can now have final designations assigned. LP 944−20 is type M9 V, BRI 0021−0214 is type M9.5 V, and PC 0025+0447 is M9.5 V (peculiar).

TABLE 6

QUALITATIVE DEFINITIONS FOR L SUBCLASSES

Subclass (1)	Spectral Characteristics[a] (2)	Example (3)
L0	VO λλ7400, 7900 at its strongest—7800–8000 Å portion of spectrum is flat TiO λ8432 depth similar to both CrH λ8611 and FeH λ8692 TiO λ7053 present at high signal-to-noise but weak Rb I and Cs I doublets weakly visible but strengthening	2MASP J0345432+254023
L1	TiO λ8432, CrH λ8611, FeH λ8692 nearly equal strength; FeH deeper than CrH, CrH deeper than TiO VO λλ7400, 7900 weakening; 7800–8000 Å portion of spectrum slightly sloped Na I doublet weakening TiO λλ7053, 8432 weakening Rb I and Cs I doublets strengthening K I line cores broadening	2MASSW J1439284+192915
L2	TiO λ8432 much weaker than CrH λ8611 or FeH λ8692; FeH deeper than CrH K I line cores still visible and still broadening TiO λ8432 weaker and TiO λ7053 vanished VO λλ7400, 7900 weakening more: 7800–8000 portion of spectrum distinctly sloped Na I weakening; Rb I and Cs I still strengthening	Kelu-1
L3	K I still broadening with cores still weakly visible VO λ7900 barely present as slight depression in "continuum" between 7800 and 8200 Å TiO λ8432 still weakening Na I still weakening; Rb I and Cs I still strengthening	2MASSW J1146345+223053
L4	K I wings are very broad and line cores no longer visible CrH λ8611 equal in strength to FeH λ8692 VO λ7900 vanished (no depression visible at all between 7800 and 8200 Å) TiO λ8432 still weakening Na I still weakening; Rb I and Cs I still strengthening	2MASSW J1155009+230706
L5	CrH λ8611 now stronger than FeH λ8692 TiO λ8432 very weak K I region shows broad depression Na I still weakening Rb I and Cs I still strengthening; Cs I λ8521 less deep than CrH λ8611	DENIS-P J1228.2−1547
L6	TiO λ8432 barely perceptible K I region shows very broad depression FeH λλ8692, 9896 and CrH λ8611 weakening; CrH λ8611 deeper than FeH λ8692 Na I still weakening Rb I and Cs I still strengthening; Cs I λ8521 now deeper than CrH λ8611	2MASSs J0850359+105716
L7	TiO λ8432 virtually gone FeH λλ8692, 9896 and CrH λ8611 still weakening; CrH λ8611 still deeper than FeH λ8692 K I region shows very broad depression Rb I and Cs I still strengthening Na I still weakening	DENIS-P J0205.4−1159
L8	FeH λλ8692, 9896 very weak CrH λ8611 still weakening though still stronger than FeH λ8692 K I region shows very broad depression Rb I and Cs I still strengthening; Cs I λ8521 ~2 times as deep as CrH λ8611 Na I barely perceptible	2MASSW J1632291+190441

[a] Relative depths of bands refer to spectra with absolute flux calibrations (F_λ) similar to those in Figs. 7 and 8.

dwarf Gl 229B shown at the bottom of Figures 6 and 7. This lends support to our belief that the coolest known L dwarfs are only slightly warmer than the temperature at which methane forms.

5.2.4. *Spectral Ratios*

In choosing classification diagnostics, we will use spectral ratios like those devised by Kirkpatrick et al. (1991). These ratios are a measure of the summed flux in a region containing a line or band of interest divided into the summed flux in a nearby region approximating the local pseudocontinuum. In Table 7 we give the name of the ratio (col. [1]), the regions used in the summing (cols. [2] and [3]), and the features being measured (col. [4]). Figures 8–12 show the ratios plotted as a function of spectral class.

Figure 8 shows spectral ratios for the alkali lines. Values for the primary standards are shown by large dots. This figure shows how the resonance lines of rubidium and cesium strengthen toward cooler types as the higher excitation sodium doublet weakens.

Figure 9 shows spectral ratios for the oxide molecules. Here, the primary standards (*large dots*) show that these TiO and VO bands reach maximum strength at very late-M types and rapidly weaken through the L sequence, disappearing completely by classes L5–L6.

Figure 10 shows spectral ratios for the hydride molecules. The CrH-a ratio for the primary standards (*large dots*) is

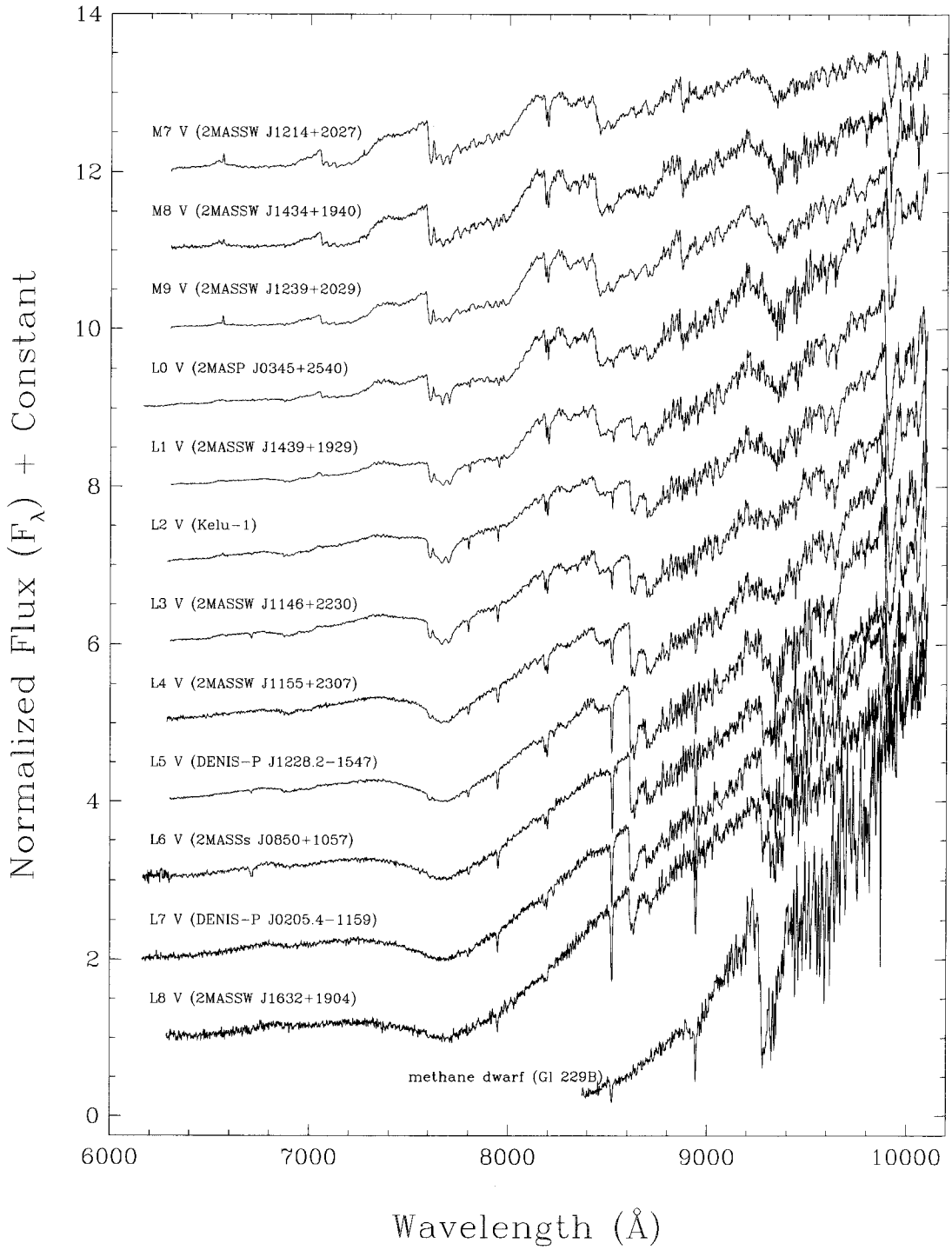

FIG. 6.—L-dwarf spectral sequence. This is a subset of the Keck LRIS data of Fig. 3, but showing only one spectrum for each subclass from L0 through L8. Also shown for comparison is the Oppenheimer et al. spectrum of Gl 229B and three late-M dwarfs from Table 1A, also taken with LRIS on Keck. Again, names for the 2MASS objects have been abbreviated.

well behaved, clearly demonstrating the fact that CrH increases strength from late M through early L, reaches peak strength at L5 V, then weakens toward the latest L types.[9] The FeH-a and FeH-b ratios show similar behavior, with FeH increasing from late M through mid-L then weakening toward the latest L types.

Because the alkalis of Figure 8 and the oxides of Figure 9 show ratios for the primary standards that monotonically increase or decrease throughout the L sequence, composite alkali-oxide ratios, which serve as more sensitive discriminants, can be devised. The values for some of these ratios are shown in Figure 11, where the primary standards are again illustrated by the large dots.

[9] As Figure 10*b* shows, the CrH-b ratio, which measures the CrH band at 9969 Å, is unusable as a spectral diagnostic in these data. This is because of the poor sensitivity of the CCD at this wavelength and because of the lack of a suitable continuum region.

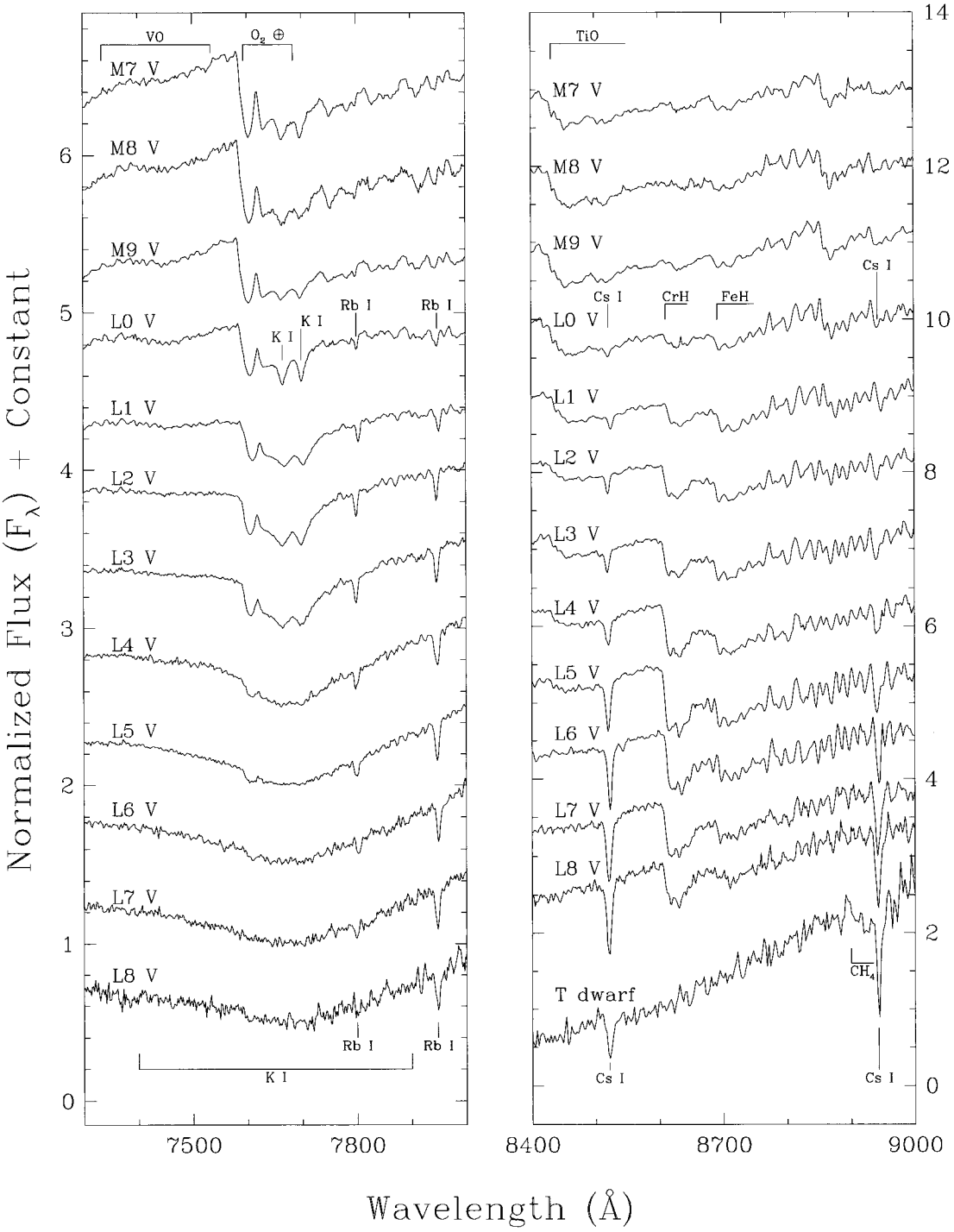

FIG. 7.—Detailed portions of the spectra from Fig. 6. Shown here are two wavelength regions that contain several diagnostics useful for spectral classification. Prominent lines and bands are marked. See § 6.2 and Table 6 for details.

Finally, ratios that measure the redness of the spectrum as a function of spectral class can be devised. Four such color ratios are shown in Figure 12, where again the primary standards are represented by the large dots. For these ratios two "continuum" points free of obvious molecular or line absorption are compared, one toward the short-wavelength end of our spectra and one toward the long-wavelength end. In all cases shown in Figure 12, however, the color ratios are very flat for types L0 through L3, then rapidly increase with cooler types beyond L3. The flatness at early L types is caused by the rapid disappearance of oxide absorption: even though cooler temperatures to first order dictate more flux at longer wavelengths, the flux at shorter wavelengths is also increasing because of the rainout of oxide molecules.

5.3. *Recipe for L-Dwarf Spectral Classification*

With the ratios of Figures 8–12 in hand, we advance the following scheme for classifying other L dwarfs. For each spectrum, the final type is determined from the strength of the hydride bands, the oxide bands, and the alkali lines along with the value of one redness ratio and the broaden-

TABLE 7

REGIONS USED IN FLUX SUMMING FOR SPECTRAL RATIOS

Ratio (1)	Numerator (Å) (2)	Denominator (Å) (3)	Feature Measured (4)
Rb-a	Av. of 7775.2–7785.2 and 7815.2–7825.2	7795.2–7805.2	Rb I λ7800.2
Rb-b	Av. of 7922.6–7932.6 and 7962.6–7972.6	7942.6–7952.6	Rb I λ7947.6
Na-a	8153.3–8163.3	8178.3–8188.3	Na I λ8183.3
Na-b	8153.3–8183.3	8189.8–8199.8	Na I λ8194.8
Cs-a	Av. of 8496.1–8506.1 and 8536.1–8546.1	8516.1–8526.1	Cs I λ8521.1
Cs-b	Av. of 8918.5–8928.5 and 8958.3–8968.3	8938.5–8948.3	Cs I λ8943.5
TiO-a	7033.0–7048.0	7058.0–7073.0	TiO λ7053
TiO-b	8400.0–8415.0	8435.0–8470.0	TiO λ8432
VO-a	Sum of 7350.0–7370.0 and 7550.0–7570.0	7430.0–7470.0	VO $\lambda \sim 7434$ Å
VO-b	Sum of 7860.0–7880.0 and 8080.0–8100.0	7960.0–8000.0	VO $\lambda \sim 7912$ Å
CrH-a	8580.0–8600.0	8621.0–8641.0	CrH λ8611
CrH-b	9940.0–9960.0	9970.0–9990.0	CrH λ9969
FeH-a	8660.0–8680.0	8700.0–8720.0	FeH λ8692
FeH-b	9863.0–9883.0	9908.0–9928.0	FeH λ9896
Color-a	9800.0–9850.0	7300.0–7350.0	Redness of spectrum
Color-b	9800.0–9850.0	7000.0–7050.0	Redness of spectrum
Color-c	9800.0–9850.0	8100.0–8150.0	Redness of spectrum
Color-d	9675.0–9875.0	7350.0–7550.0	Redness of spectrum

TABLE 8A

VALUES OF SPECTRAL DIAGNOSTICS FOR THE SPECTRA IN FIGURE 7

Object Name (1)	Type (2)	CrH-a (3)	Rb-b/TiO-b (4)	Cs-a/VO-b (5)	Color-d (6)
2MASSW J1214063+202702	M7 V	0.996	0.649	0.867	2.793
2MASSW J1434264+194050	M8 V	1.034	0.588	0.795	3.725
2MASSW J1239194+202952	M9 V	1.043	0.576	0.736	5.345
2MASP J0345432+254023	L0 V	1.161	0.662	0.781	6.654
2MASSW J1439284+192915	L1 V	1.371	0.812	0.856	7.333
Kelu-1	L2 V	1.537	1.048	1.029	6.700
2MASSW J1146345+223053	L3 V	1.636	1.155	1.125	7.210
2MASSW J1155009+230706	L4 V	1.909	1.323	1.258	9.713
DENIS-P J1228.2−1547	L5 V	2.203	1.658	1.488	14.406
2MASSs J0850359+105716	L6 V	1.786	1.703	1.561	15.549
DENIS-P J0205.4−1159	L7 V	1.551	2.189	1.604	22.027
2MASSW J1632291+190441	L8 V	1.289	2.564	1.626	30.015

TABLE 8B

VALUES OF SPECTRAL DIAGNOSTICS FOR OTHER L DWARFS

Object Name (1)	CrH-a (2)	Rb-b/TiO-b (3)	Cs-a/VO-b (4)	Color-d (5)	K I Fit (6)	Final Type (7)
2MASSW J0147334+345311	1.281(0–1)	0.750(0–1)	0.830(0–1)	...	(0–1)	L0.5 V
2MASSW J1439409+182637	1.283(0–1)	0.849(1)	0.884(1)	...	(1)	L1 V
2MASSW J1145572+231730	1.465(1–2)	1.030(2)	0.996(2)	...	(1–2)	L1.5 V
2MASSW J0242435+160739	1.356(1)	0.982(2)	0.942(1–2)	...	(1–2)	L1.5 V
2MASSW J1334062+194034	1.591(2)	0.937(1–2)	0.965(1–2)	...	(1–2)	L1.5 V
2MASSW J0030438+313932	1.504(2)	0.991(2)	0.952(1–2)	...	(2)	L2 V
2MASSW J1342236+175156	1.518(2)	1.102(2–3)	1.070(2–3)	...	(2–3)	L2.5 V
2MASSW J0918382+213406	1.494(2)	1.184(3)	1.063(2–3)	...	(2–3)	L2.5 V
DENIS-P J1058.7−1548	1.789(3–4)	1.165(3)	1.146(3)	...	(3)	L3 V
2MASSW J0913032+184150	1.710(3)	1.152(3)	1.094(3)	...	(3)	L3 V
2MASSW J0355419+225702	1.681(3)	1.188(3)	1.085(3)	...	(3)	L3 V
2MASSW J0326137+295015	1.668(3)	1.279(3–4)	1.214(3–4)	...	(3)	L3.5 V
2MASSW J0129122+351758	1.864(4)	1.326(4)	1.293(4)	...	(4)	L4 V
GD 165B	1.875(4)	1.496(4–5)	1.289(4)	...	(3)	L4 V
2MASSW J1328550+211449	1.967(∼5)	1.661(5)	1.233(4)	14.326(5)	...	L5 V
2MASSW J1553214+210907	1.904(5–6)	1.755(6)	1.472(5)	11.841(5)	...	L5.5 V

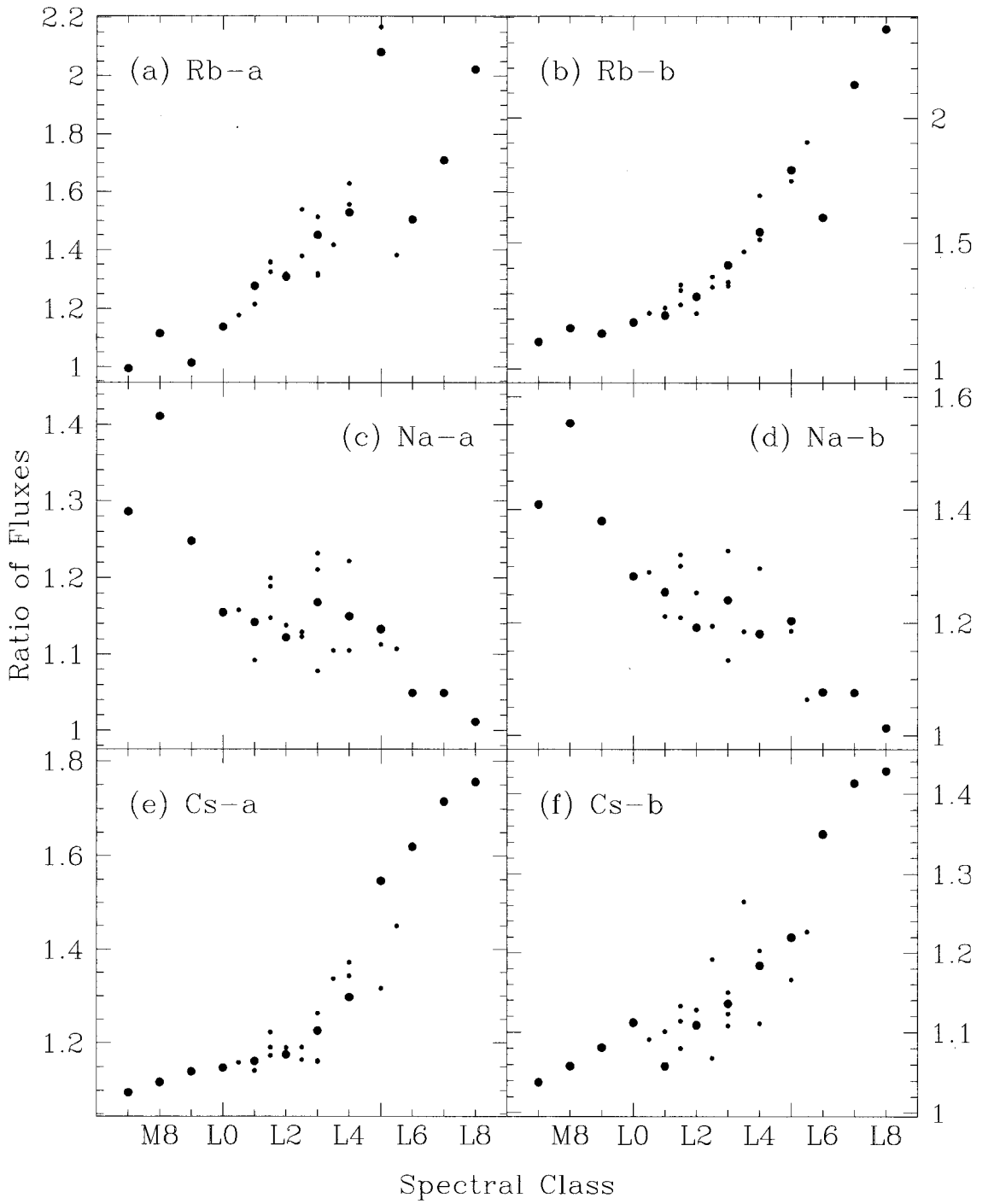

FIG. 8.—Spectral ratios for the alkali lines, as defined in Table 7. The L-dwarf primary standards along with the three M dwarfs from Fig. 7 are shown by the large dots. The other L dwarfs are shown as smaller dots, calculation of their final spectral types being described in § 5.3.

ing of the potassium doublet (which is a by-eye best fit to the K I profiles of the primary standards). For these we choose the best-behaved ratios shown in Figures 8–12.

Specifically, for the hydride measure we choose CrH-a from Figure 10. For the oxide and alkali measures, we choose the two best composite ratios from Figure 11: Rb-b/TiO-b and Cs-a/VO-b. For the redness criterion we choose the color-d ratio from Figure 12. The actual values of these ratios for the primary standards are given in Table 8A.

The two alkali-oxide ratios monotonically increase throughout the L sequence. The CrH-a ratio is very sensitive though nonmonotonic—proper use of this ratio requires a preliminary classification from the alkali-oxide ratios. The final two diagnostics—the redness ratio and the K I broadening—are usable over different parts of the L sequence. Because the redness ratios are flat between L0 and L4, these provide meaningful criteria only for types L5 and cooler. Likewise, as seen from Figure 7 the broadening of the K I lines is most sensitive for types warmer than L5. In total, then, four ratios will be used to determine L-dwarf classifications: CrH-a, Rb-b/TiO-b, Cs-a/VO-b, and either color-d (types $\geq$ L5) or the K I fit (types $<$ L5).

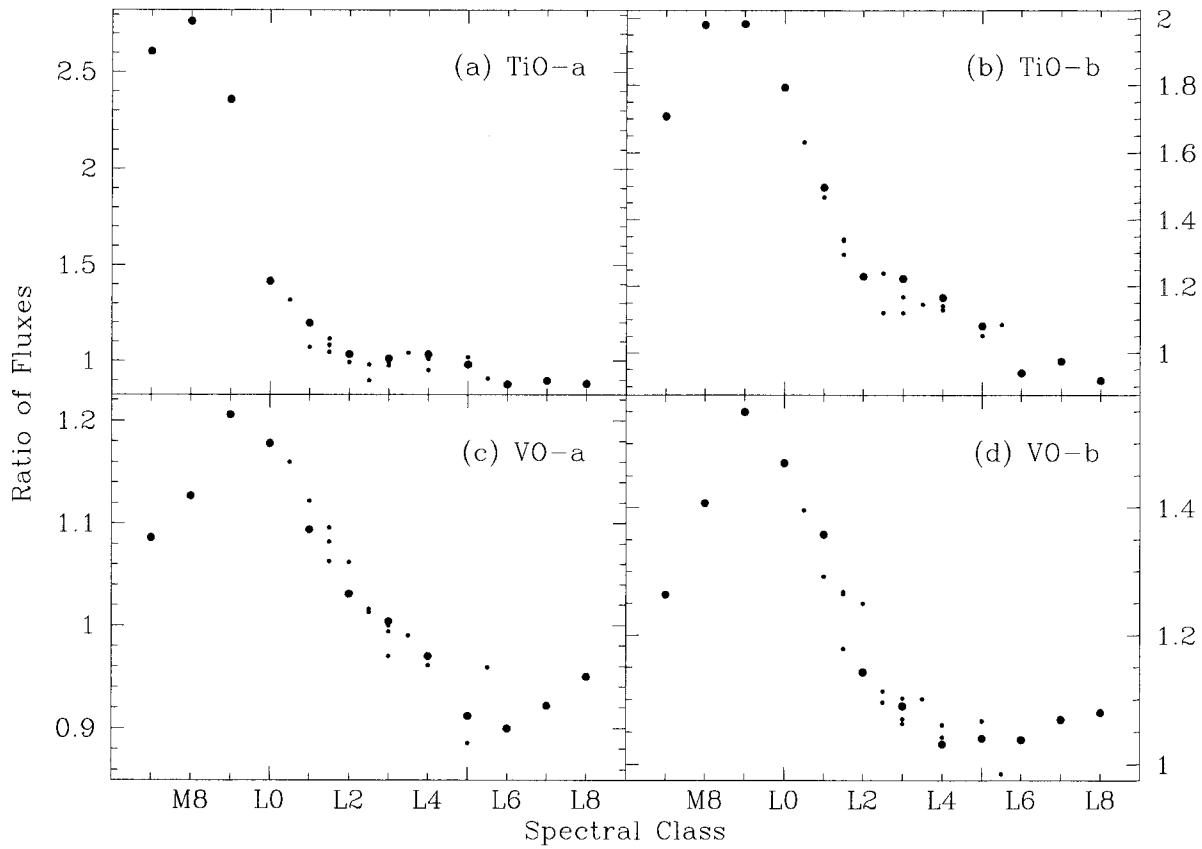

FIG. 9.—Same as Fig. 8 except showing the oxide ratios defined in Table 7

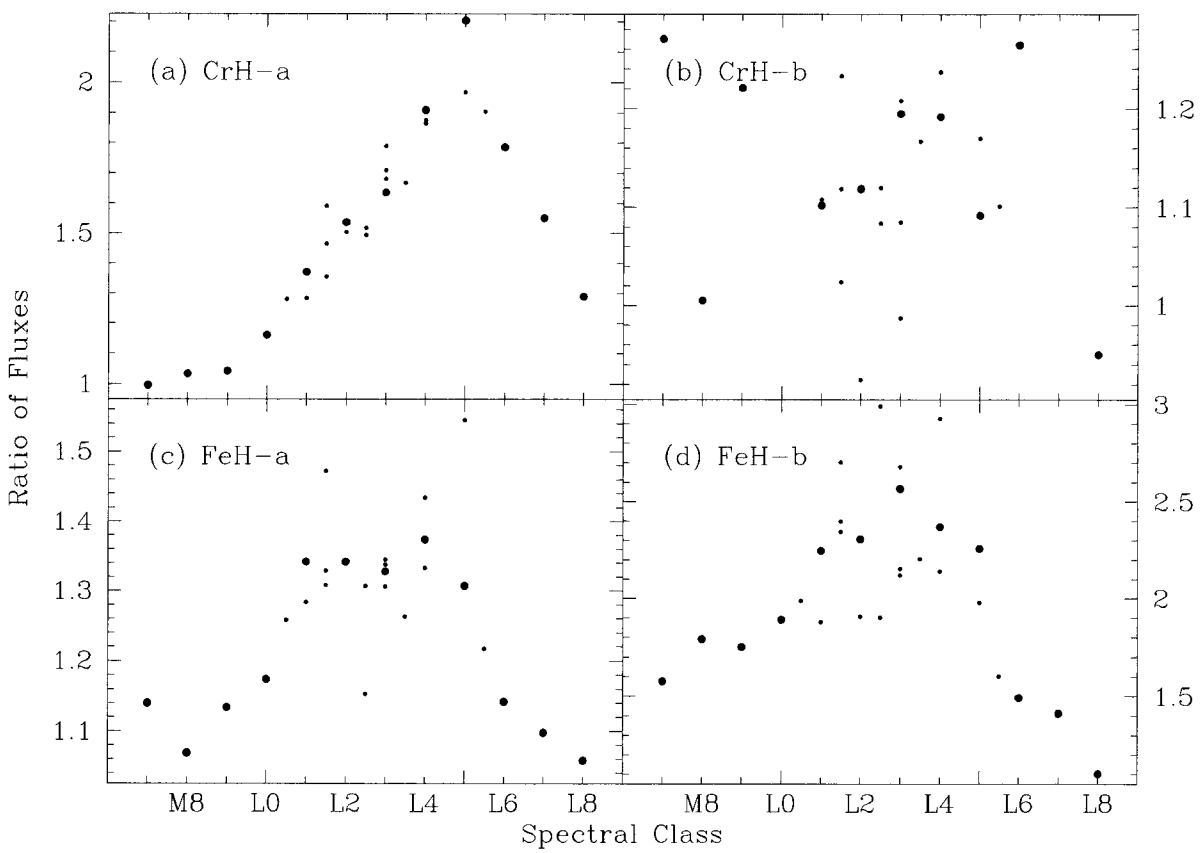

FIG. 10.—Same as Fig. 8 except showing the hydride ratios defined in Table 7

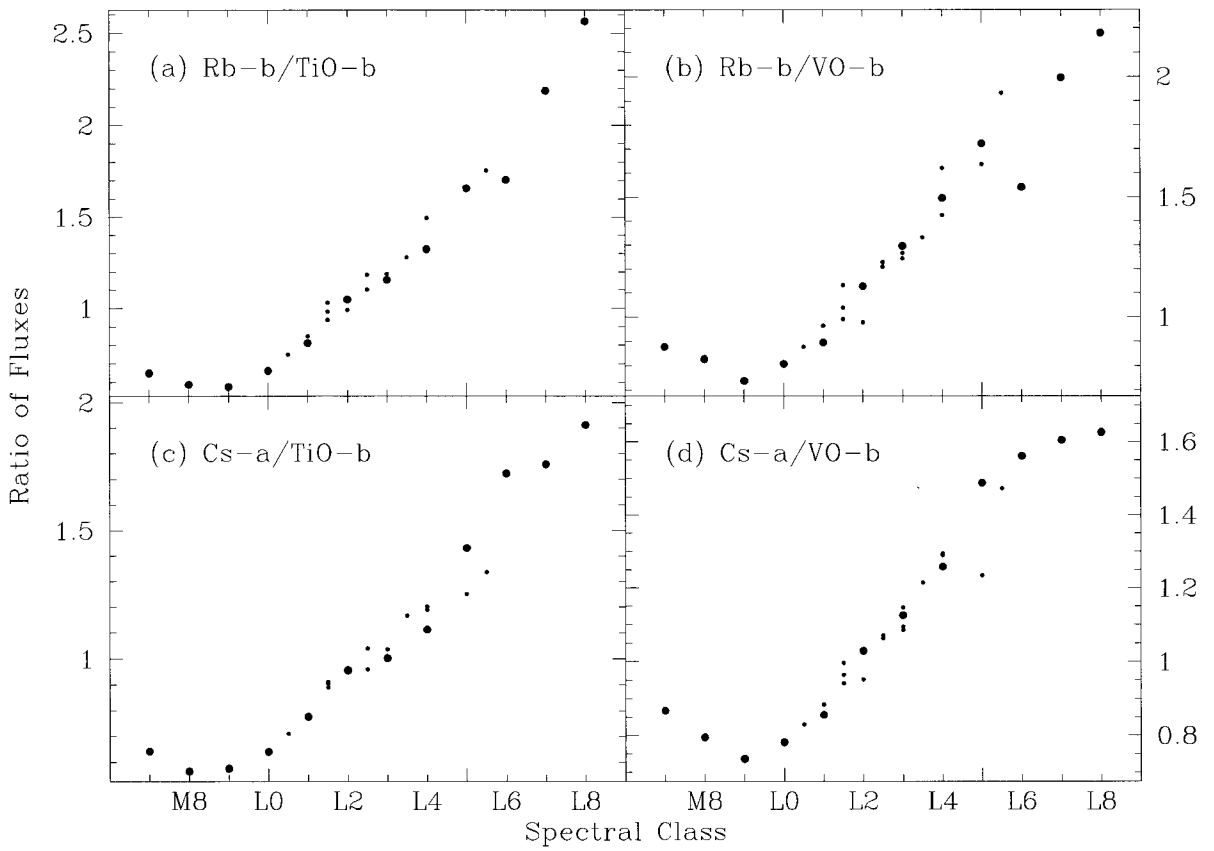

FIG. 11.—Same as Fig. 8 except showing the composite alkali/oxide ratios from Table 7

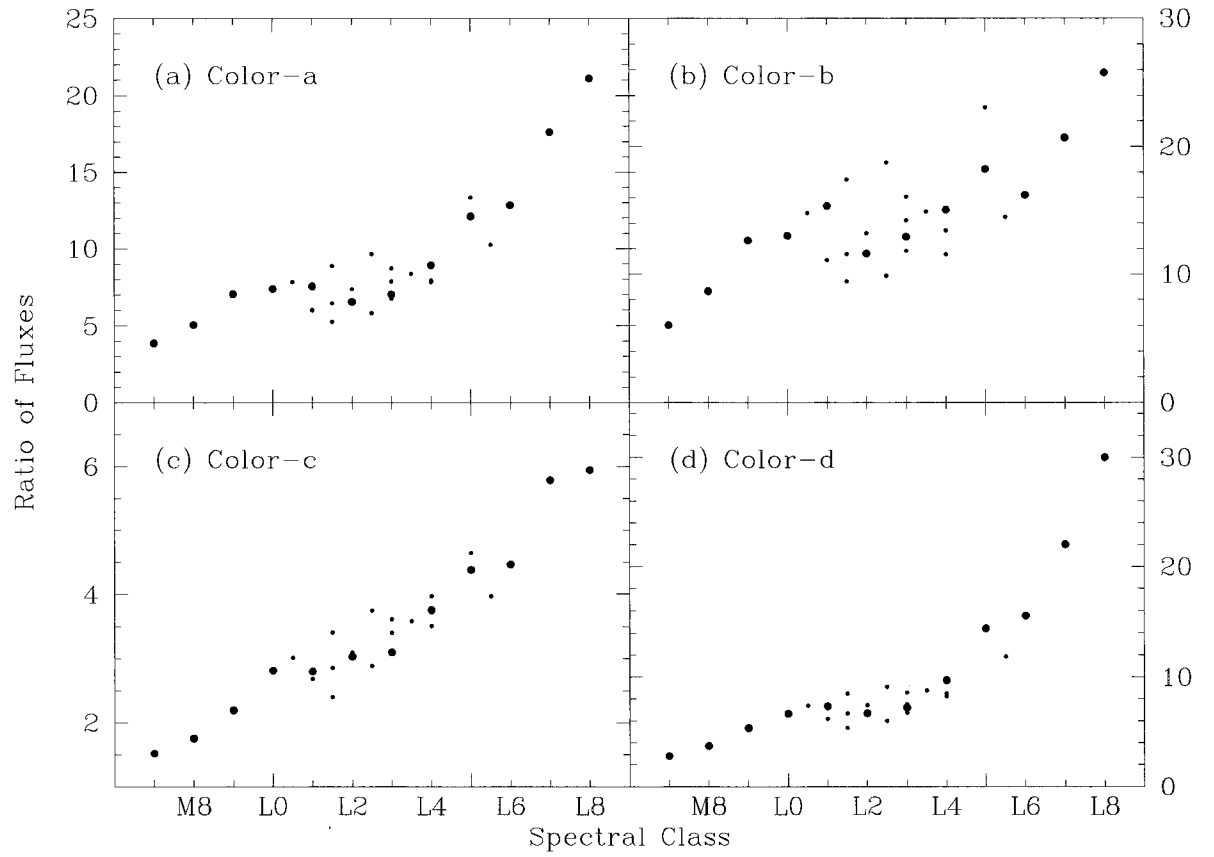

FIG. 12.—Same as Fig. 8 except showing the color ratios defined in Table 7

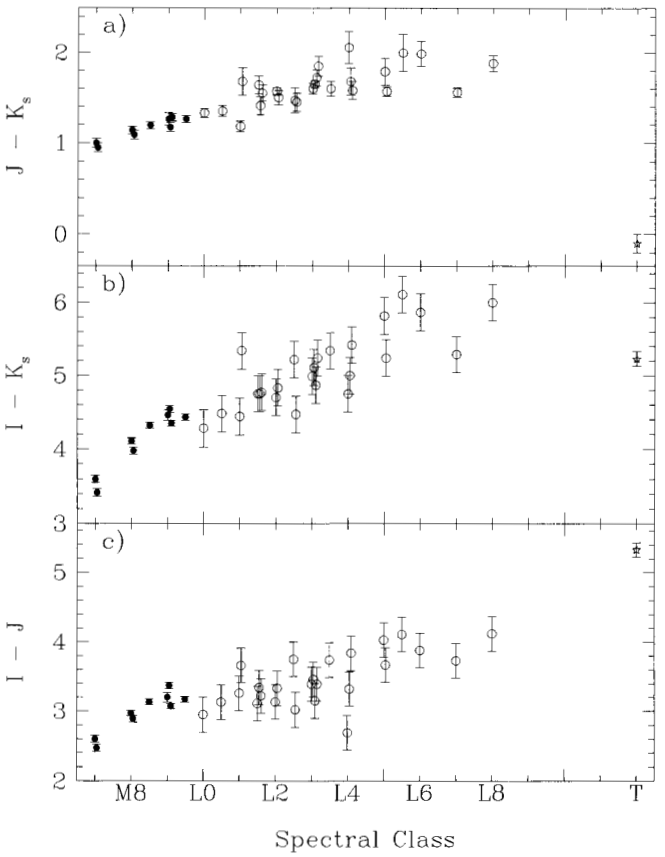

FIG. 13.—(*a*) Plot of the 2MASS-measured $J-K_s$ color vs. spectral class for the L dwarfs of Table 3 (*open circles*). Also shown for comparison are late-M dwarfs (*filled circles*) from Tinney et al. (1993) and Leggett (1992) along with Gl 229B (*open star*). From late M through the L sequence there is a general trend of redder color with later spectral type, although the scatter at any given L class is on the order of ~0.3 mag. Note however the abrupt change in color caused by the onset of methane absorption at K_s in Gl 229B. (*b*) Same as (*a*), except showing $I-K_s$ colors where the I magnitudes for the L dwarfs are measured directly off the LRIS spectra. Again, there is a monotonic trend (with some scatter) from late M through the L sequence. (*c*) Same again, except for the $I-J$ color. Because neither the I nor the J band is affected by methane absorption, the $I-J$ color increases monotonically over the entire range from late M through type T.

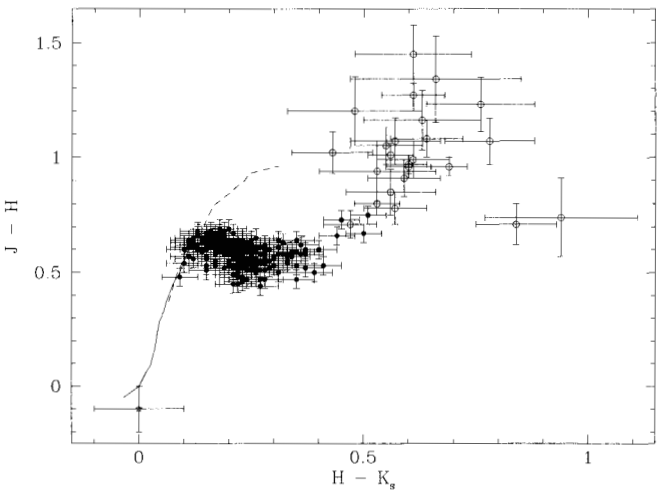

FIG. 14.—$J-H$ vs. $H-K_s$ diagram for M and L dwarfs. The M dwarfs (*filled circles*) are from Leggett (1992), and the L dwarfs (*open circles*) are from this paper. The position of Gl 229B is shown by an open star. Tracks for dwarfs (*solid line*) and giants (*dashed line*) from Bessell & Brett (1988) are also shown.

Values of these ratios for the other L dwarfs are given in Table 8B. In parentheses after each value is the L type to which that value most closely corresponds as judged from the relation determined from the primary L-dwarf standards. In some cases, the value falls midway between two standard types, so a type such as "2–3" is given. The median of types given by all four ratios is then the final type. These final types are given in the last column of Table 8B.

6. FURTHER DISCUSSION ON L-DWARF SPECTRA

6.1. *Colors*

The plot of 2MASS $J-K_s$ colors versus final spectral type is shown in Figure 13*a*. Data for a few late-M dwarfs from Tinney, Mould, & Reid (1993) and Leggett (1992) are shown for comparison.[10] Also shown is the location of the only known T dwarf, Gl 229B. The plot shows that the $J-K_s$ color is, with some cosmic scatter, monotonically increasing with later type from late M through late L then turns dramatically bluer for Gl 229B once methane absorption starts to dominate the K_s-band measurement.

Using the absolute flux calibration of the Keck spectra, we can derive rough I-band measurements for each of the L dwarfs as well. Specifically, we have taken a simple square bandpass with beginning and end points lying at the half-power points of the I_C band (7250 and 8750 Å; Bessell 1979) and have calculated the average flux in units of F_ν (ergs cm^{-2} s^{-1} Hz^{-1}) in the bandpass. Using a zero-point flux of 2550 Jy for the I_C filter (Berriman & Reid 1987), we have converted these fluxes to magnitudes and listed the results along with the $I-K_s$ colors in columns (6) and (7) of Table 3. The $I-K_s$ color is shown as a function of spectral type in Figure 13*b*, again with late-M dwarfs and Gl 229B for comparison. Note that $I-K_s$ increases fairly monotonically with spectral type for L dwarfs, meaning that a crude type can be assigned based on the $I-K_s$ color alone. However, this trend reverses by the time temperatures like that of Gl 229B are encountered.

Figure 13*c* shows $I-J$ color as a function of spectral type. Because neither the I nor J bands are directly affected by methane absorption, the $I-J$ color increases monotonically from late-M through T types.

The 2MASS color can also be used to plot L dwarfs on the familiar $J-H$ versus $H-K_s$ diagram. This is shown in Figure 14. For illustration, M dwarfs from Leggett (1992) are also plotted together with Gl 229B and the tracks for giants (*dashed line*) and dwarfs (*solid line*) from Bessell & Brett (1988). For the most part, L dwarfs lie on a redward extension of the well-known dwarf track.[11] Note however the position of Gl 229B on the opposite side of the diagram from the L dwarfs.

[10] These publications list K_{CIT} photometry, not K_s. However, Persson et al. (1998) have shown that for late-M dwarfs the difference between K and K_s is negligible.

[11] The points for 2MASSW J1439409+182637 and 2MASSW J1334062+194034 lie outside the locus defined for the other L dwarfs. It is not yet known if this is a real effect or simply an indication of H-band photometry possibly biased by strong OH airglow in the 2MASS measurements.

TABLE 9

EQUIVALENT WIDTH MEASUREMENTS FOR THE DWARFS IN TABLE 3

Object Name (1)	Spectral Type (2)	Hα Emission 6563 Å EW (Å) (3)	Li I Absorption 6708 Å EW (Å) (4)	Rb I Absorption 7948 Å EW (Å) (5)	Cs I Absorption 8521 Å EW (Å) (6)
2MASP J0345432+254023	L0 V	≤0.3	<0.5	2.7	1.5
2MASSW J0147334+345311.....	L0.5 V	<0.5	<1.0	2.7	1.8
2MASSW J1439284+192915.....	L1 V	<0.3	<0.3	3.2	1.8
2MASSW J1439409+182637.....	L1 V	<0.6	5.6	3.5	2.0
2MASSW J1145572+231730.....	L1.5 V	4.2	<0.4	3.5	2.1
2MASSW J0242435+160739.....	L1.5 V	<0.5	<0.7	2.9	2.1
2MASSW J1334062+194034.....	L1.5 V	4.2	<1.5	2.8	3.1
Kelu-1.....	L2 V	1.9	1.7	2.8	2.0
2MASSW J0030438+313932.....	L2 V	4.4	<1.0	2.9	2.3
2MASSW J1342236+175156.....	L2.5 V	<2.2	≤3.9	3.3:	1.8
2MASSW J0918382+213406.....	L2.5 V	<0.3	<0.3	3.2	2.2
2MASSW J1146345+223053.....	L3 V	≤0.3	5.1	3.7	2.4
DENIS-P J1058.7−1548.....	L3 V	1.6	<0.3	3.4	2.8
2MASSW J0913032+184150.....	L3 V	<0.8	<1.0	3.2	2.2
2MASSW J0355419+225702.....	L3 V	<0.5	<1.3	3.0:	2.6:
2MASSW J0326137+295015.....	L3.5 V	9.1	<1.0	4.0	3.1
2MASSW J0129122+351758.....	L4 V	<0.5	3.3	4.4	3.6
2MASSW J1155009+230706.....	L4 V	<1.0	<0.5	4.6	3.1
GD 165B	L4 V	<0.8	<0.7	4.6	3.1
2MASSW J1328550+211449.....	L5 V	<2.0	<3.0	6.6:	3.8
DENIS-P J1228.2−1547.....	L5 V	≤0.6	3.1	5.5	4.4
2MASSW J1553214+210907.....	L5.5 V	<4.3	18.5	8.1:	5.0
2MASSs J0850359+105716	L6 V	<0.9	15.2	4.9	4.7
DENIS-P J0205.4−1159.....	L7 V	<2.7	<1.3	6.8	5.7
2MASSW J1632291+190441.....	L8 V	≤4.0	≤9.4	6.9	5.6
Gl 229B.....	T dwarf	...	...	...	5.9

NOTE.—Equivalent widths (EWs) have typical errors of ±0.2 Å for most of the spectra presented here, but those with poorer signal-to-noise ratios have errors of around ±0.5 Å.

6.2. Hα *Emission*

Several of the L dwarfs in Table 3 exhibit Hα in emission. Equivalent width (EW) measures are listed in column (3) of Table 9 and are plotted as a function of spectral class in Figure 15*a*. Those spectra with clear or possible Hα emission are shown in Figure 16. The coolest object with measurable Hα, 2MASSW J0326137+295015, also has the strongest line: 9.1 Å EW.[12]

6.3. *Lithium Absorption*

Seven of the 25 L dwarfs show the Li I 6708 Å line in our LRIS spectra. Two of these are previously known brown dwarfs—Kelu-1 and DENIS-P J1228.2−1547. The other five are all 2MASS discoveries. Two other 2MASS L dwarfs may have lithium at our detection limit. Equivalent width measures are listed in column (4) of Table 9 and are plotted as a function of spectral type in Figure 15*b*. Those spectra with clear or possible lithium signatures are shown in Figure 17. Note that two of the 2MASS objects have Li I in excess of 15 Å EW. Lithium is discussed more fully in § 8.3.

6.4. *Rubidium and Cesium Absorption*

Figures 15*c* and 15*d* show the equivalent width measurements for Rb I and Cs I as a function of spectral class. Values are listed in columns (5) and (6) of Table 9. For Rb I, only the line at 7948 Å was measured since the line at 7800 Å falls in a low signal-to-noise ratio region in the latest L dwarfs, making the EW measurements here more uncertain. For Cs I, only the line at 8521 Å was measured since the line at 8943 Å is contaminated by telluric absorption. For both rubidium and cesium, the EWs are seen to increase for cooler L dwarfs, making these excellent measures of spectral type. However, measuring these EWs is possible only because these spectra have good signal-to-noise ratios and because these two lines lie in fairly unconfused regions of the spectrum where a pseudocontinuum can be readily determined. For general classification, the composite alkali-oxide ratios described in § 5.2.4 should be used instead.

7. TRIGONOMETRIC PARALLAXES FOR L DWARFS

Five of the objects in Table 3 have measured trigonometric parallaxes. Two of these have been previously published (GD 165B and Gl 229B), but the other three are new results from the US Naval Observatory (USNO) parallax program described in Monet et al. (1992). Table 10 lists these five objects and their spectral types (cols. [1] and [2]) along with their proper-motion vectors (cols. [3] and [4]) and parallax determinations (col. [5]). References for the parallax values are given in column (6). Finally, absolute J, H, and K_s magnitudes are given in columns (7)–(9). Note that the absolute J magnitude for the L7 dwarf is 1.7 mag dimmer than that of the L0 dwarf yet 2.0 mag brighter still than that of Gl 229B.

Because we now have absolute magnitudes that sample the L-dwarf sequence for types L0, L1, L4, and L7, we can

[12] However, the M9.5 dwarf 2MASSW J0149090+295613 is only slightly warmer than the earliest L dwarf and it has been observed during a massive flare in which the Hα EW was hundreds of angstroms. See Appendix B for more on this object.

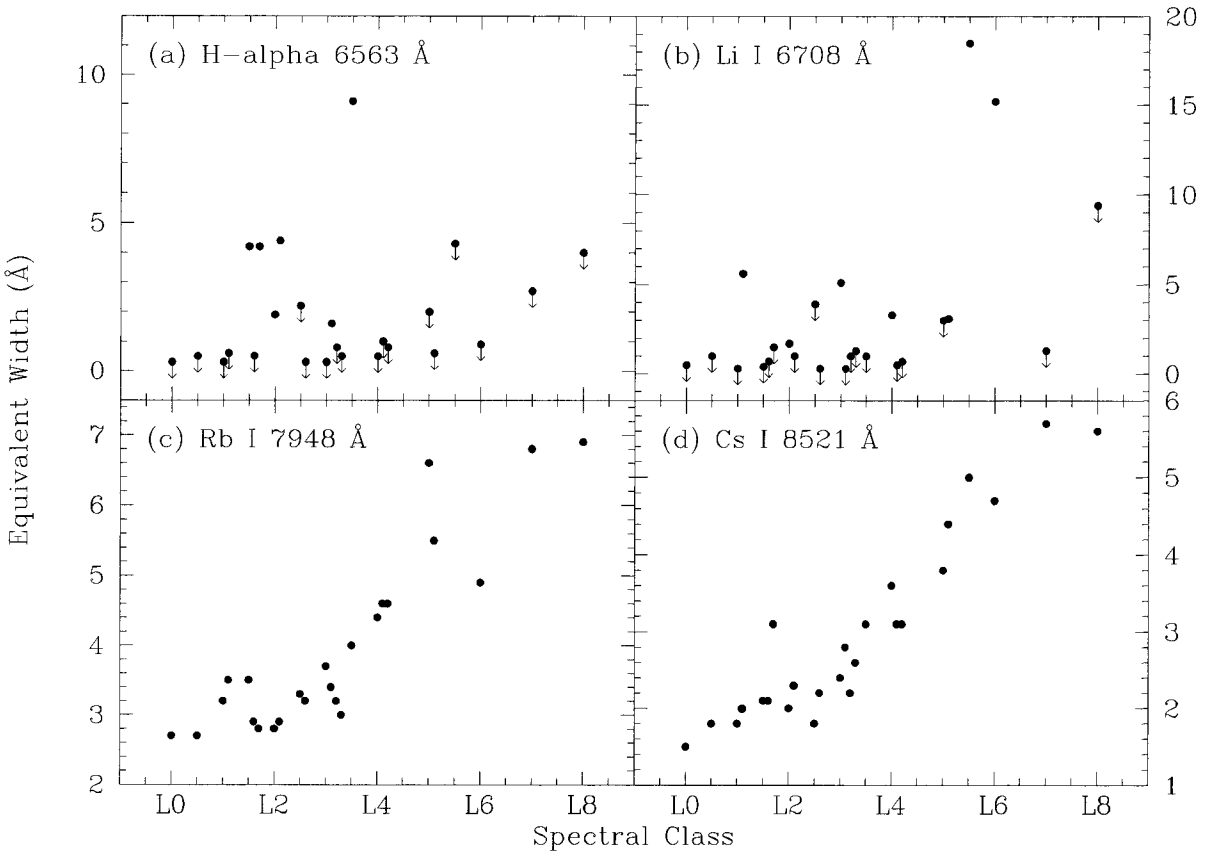

FIG. 15.—Equivalent width measures for all 25 L dwarfs as tabulated in Table 9. (*a*) Hα emission strength; (b) Li I strength; (*c*) Rb I strength; and (*d*) Cs I strength. Downward-pointing arrows indicate upper limits. Equivalent widths have typical errors of ±0.2 Å, but for poorer signal-to-noise ratio spectra the errors can be around ±0.5 Å.

interpolate to other L types and thus compute spectrophotometric distance estimates for those objects in Table 3 lacking trigonometric parallaxes. The distance estimates are listed in column (8) of Table 3, and an asterisk in that column indicates an object currently on the USNO parallax program. These estimates show that ~25% of the L dwarfs discovered so far are close enough ($d \leq 25$ pc) for inclusion in the Catalog of Nearby "Stars" (Gliese & Jahreiss 1991).

8. L-DWARF PHYSICS

8.1. *A Qualitative View of L-Dwarf Atmospheres*

The early atmospheric calculations of Allard (1990; see also Burrows & Liebert 1993) show that at red wavelengths TiO dominates the opacity of M dwarfs. H^- and H_2^- are also important, though decreasing in importance at cooler M types as the electron density decreases with $T_{\rm eff}$. At the end of the M sequence, TiO has begun to weaken while VO is reaching maximum strength. These are the dominant absorbers at these wavelengths, and they hide individual atomic lines. Moderate spectral resolution is required to resolve the Na I D resonance doublet amidst the TiO, while high resolution is required to detect the Li I lines in a young object (at ≤1 Å EW). The formation of dust can also veil molecular features, which may partly explain why TiO begins to weaken in the latest M dwarfs. Moreover, calculations by Burrows & Sharp (1999) show that TiO begins to condense out at temperatures less than about 2350K, corresponding roughly to spectral type M7 V.

Beginning with early-L dwarfs, VO weakens and TiO fades dramatically in the red, resulting in a spectrum qualitatively different from those of M stars. Molecular equi-

TABLE 10

OBJECTS FROM TABLE 3 WITH TRIGONOMETRIC PARALLAXES

Object Name (1)	Spectral Type (2)	μ (arcsec yr^{-1}) (3)	θ (deg) (4)	$\pi_{\rm trig}$ (arcsec) (5)	Reference (6)	M_J (mag) (7)	M_H (mag) (8)	M_{K_s} (mag) (9)
2MASP J0345432+254023	L0 V	0.104 ± 0.001	249.4 ± 0.9	0.0355 ± 0.0008	1	11.78	10.98	10.45
2MASSW J1439284+192915.....	L1 V	1.297 ± 0.066	288.7 ± 1.0	0.0648 ± 0.0033	1	11.82	11.11	10.64
GD 165B[a]	L4 V	0.256 ± 0.001	235.8 ± 0.2	0.0317 ± 0.0025	1,2	13.2	12.3	11.7
DENIS-P J0205.4−1159.....	L7 V	0.436 ± 0.005	83.1 ± 0.4	0.0601 ± 0.0032	1	13.44	12.48	11.88
Gl 229B[a]	T dwarf	0.727 ± 0.001	190.9 ± 0.1	0.1732 ± 0.0011	3	15.4	15.5	15.5

[a] Proper motion and parallax are those measured for the brighter A component.

REFERENCES FOR MOTIONS AND PARALLAXES.—(1) this paper; (2) van Altena, Lee, & Hoffleit 1995; (3) *Hipparcos*.

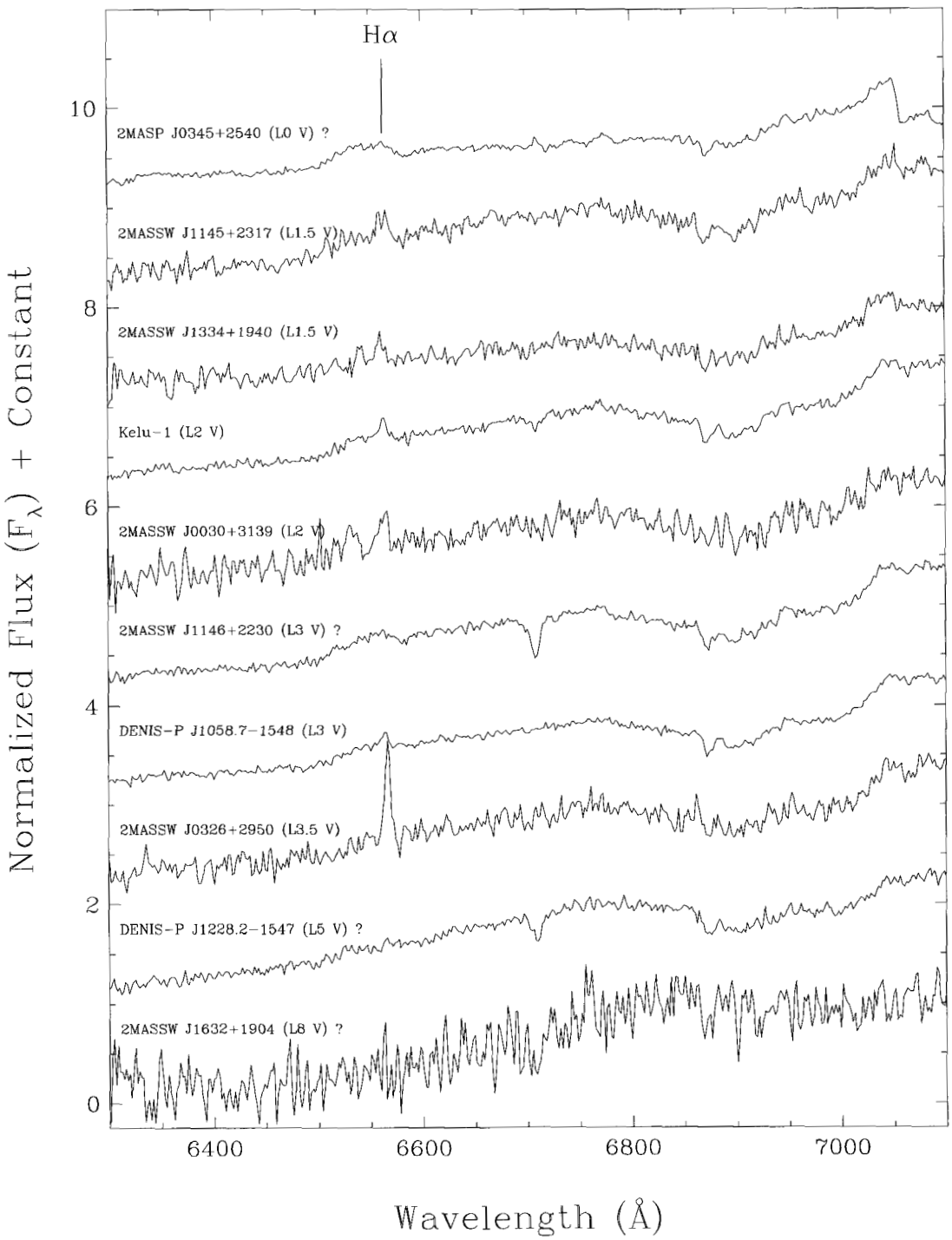

FIG. 16.—Detailed portions of the spectra near the Hα emission line for those objects with Hα detections or possible Hα detections, the latter labeled with question marks (see Table 9).

librium calculations (Burrows & Sharp 1999) show that all of the several major absorbers in this wavelength region decline rapidly with decreasing $T_{\rm eff}$. The molecular strengths decline because the molecules condense out onto grains, and the H^- and H_2^- opacities decline because there are even fewer electron donors at these low temperatures. As a consequence the red spectral region changes from being one that is very opaque to one that is quite transparent to emerging radiation. As a result, the remaining atomic lines—the Na I, K I, Rb I, and Cs I doublets—appear more strongly because of less overall absorption at these wavelengths. In other words, the characteristic late-M spectrum with occasional pseudocontinuum windows between deep flux minima gives way to a simple rising red continuum with only a few hydride molecules and atomic lines.

Perhaps the most dramatic feature, and one that strengthens throughout the L spectral sequence, is the broadening of the K I resonance doublet, which for the latest L types becomes hundreds of angstroms wide—at least as wide as the lines in cool white dwarf atmospheres

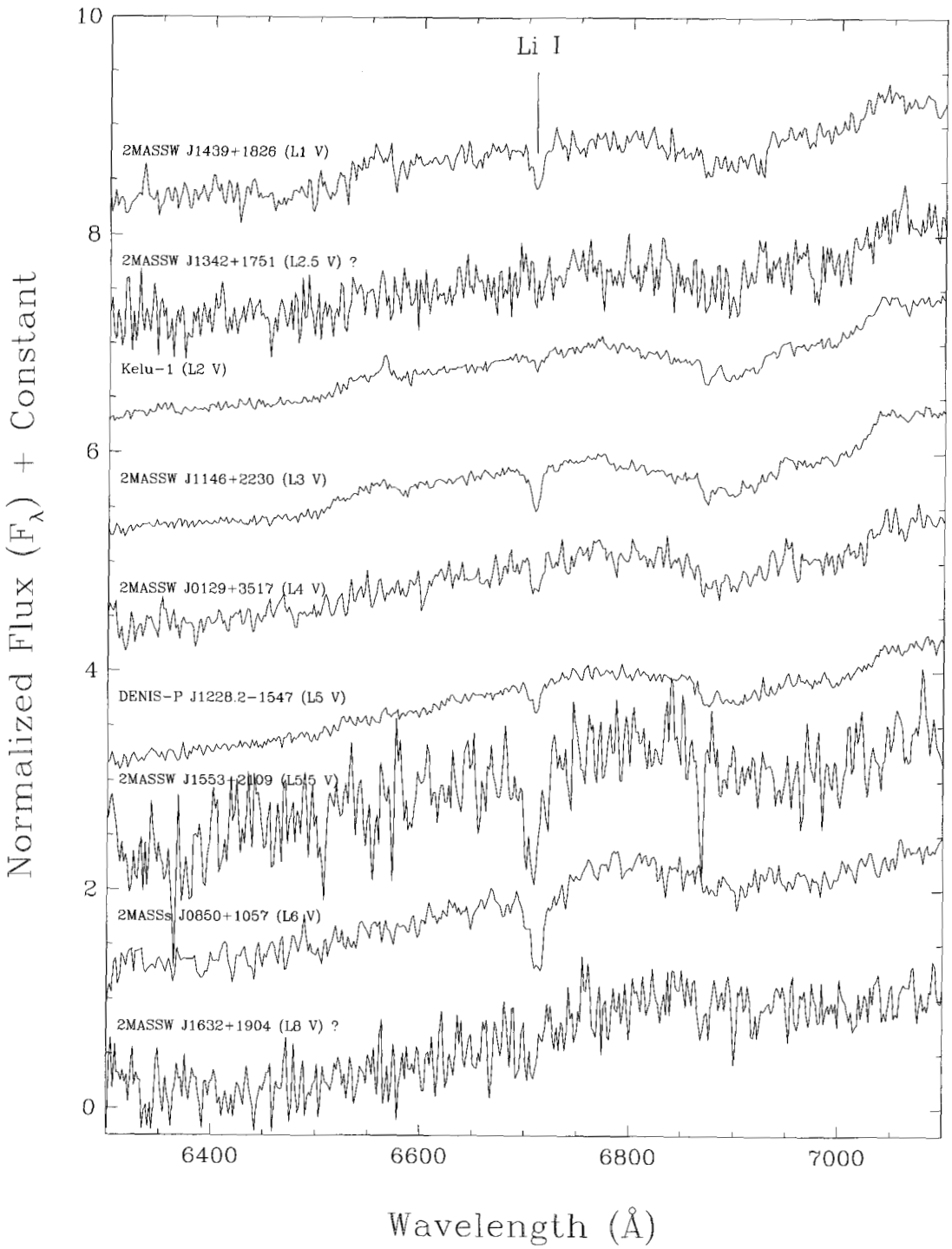

FIG. 17.—Detailed portions of the spectra near the Li I line for those objects with lithium detections or possible lithium detections, the latter labeled with question marks (see Table 9).

(although white dwarfs have log $g \approx 8$ and these objects have log $g \approx 5$). The other neutral alkali lines in our wavelength regime do not behave in this way.

Why is K I unique? At these low temperatures, almost all of the alkali atoms will be in their ground state. Of the five alkali doublets in our spectra, all but Na I at 8183, 8195 Å are ground-state transitions (see Table 4). Excepting sodium then, potassium has by far the highest solar abundance—when normalized to the number of hydrogen atoms [N(H) = 2.79 × 10^{10}], Li has 57, K has 3770, Rb has 7.09, and Cs has 0.372 (Anders & Grevesse 1989). (On the same scale, Na has 57400.) As the atmospheres of L dwarfs become more and more transparent at cooler types, the column density of potassium increases to the point where the wings of the absorption lines become damped. The surface gravities of these objects also dictate that pressure broadening must play a role in shaping the wings. This remarkable broadening of the K I doublet is predicted by the models of Allard and collaborators, as shown in the paper by Tinney et al. (1998).

TABLE 11

SPECTRAL FEATURES USABLE AS L-DWARF TEMPERATURE INDICATORS

Atom or Molecule (1)	Observed Maximum (2)	Observed Disappearance (3)	Theoretical Explanation[a] (4)	Predicted Disappearance[a] (5)
TiO	~M8	~L2[b]	Condenses into $CaTiO_3$	2300–2000 K
VO	~M9	~L4	Depletes into solid VO	1700–1900 K
FeH	~L4	>L8	...[c]	...[c]
CrH	~L5	>L8	Converts into metallic CrH	~1400 K
Li I	~L6?	~L7?	Forms into LiCl	≤1400 K
CO	...	...	C becomes bound to CH_4	1200–1500 K
Rb I	≥L8	...	Forms into RbCl	≤1200 K
Cs I	≥L8	...	Forms into CsCl	≤1200 K
K I	...	...	Forms into KCl	≤1200 K
Na I[d]	...	...	Forms into NaCl	~1150 K
H_2O	...	...	Disappears into H_2O condensate	~350 K

[a] Taken from Burrows & Sharp 1999.

[b] True for all bands except the one at 8432 Å, which doesn't disappear until about L5–6.

[c] Not included in Burrows & Sharp 1999.

[d] Only a higher excitation doublet, not the ground-state doublet, is included in our spectral region. See text for discussion.

If this scenario is correct, then the ground-state transition of Na I—the D doublet at 5890, 5895 Å—should begin to broaden at earlier spectral types than K I since sodium has an even higher abundance. The spectra presented here do not probe blueward of 6300 Å, mainly because of the futility of observing in a region where so little flux emerges. However, this spectral region has been published for one bright L dwarf—Kelu-1. As this 3750–6900 Å spectrum shows (Ruiz et al. 1997), the Na D doublet is several hundred angstroms wide—wider than the K I doublet in the same object—just as predicted. This is also confirmed in a new 2MASS discovery that is estimated to be as close as Kelu-1 but roughly two L subtypes cooler (Reid et al. 1999b).

8.2. *The Temperature Scale for L Dwarfs*

Using the spectral diagnostics shown in Figures 8, 9, and 10 along with the atmospheric properties predicted by Burrows & Sharp (1999), a rough ab initio temperature scale can be assigned to the L spectral sequence. Table 11 gives the major spectroscopic features (col. [1]) seen in the spectra of Figures 5 and 7 and indicates where in spectral type the feature reaches maximum strength (col. [2]) and where it disappears from the observed spectra (col. [3]). Column (4) lists the theoretical reason that the feature disappears, and column (5) gives the temperature at which it is expected to vanish from the spectrum. Generally, these disappearances are triggered by depletion into grains (for the molecules) or by formation into a chloride compound (for the alkali atoms). The rows of Table 11 are ordered so that features that are observed to disappear at the warmest temperatures are listed at the top, and those disappearing at cooler temperatures are at the bottom.

The first feature to disappear is titanium oxide. It slowly vanishes from the photosphere as it condenses into grains of perovskite ($CaTiO_3$). All bands of TiO have disappeared by L2 V except for the one at 8432 Å. As seen in Table 4, this band is the only TiO band not arising from the $A\ ^3\Phi$–$X\ ^3\Delta$ transition. Presumably, this transition originates at deeper layers in the photosphere and is the last to vanish as the photosphere becomes more transparent, largely through the disappearance of TiO at higher levels. This change in the physical location of the photosphere ($\tau = 1$) makes it difficult to ascribe the spectral type at which TiO truly disappears. Nonetheless, the observed maximum in TiO absorption around M7–8 V suggests that the 2300–2000 K regime lies at somewhat later spectral types, probably very early L.

Vanadium oxide is a little less problematic. After reaching a maximum at ~M9.5 V, it vanishes from the spectrum by ~L4 V after depleting onto solid VO.[13] Thus, L4 V roughly marks the 1700–1900 K regime.

The next feature to weaken and disappear is Na I. After reaching a maximum in the M dwarfs, sodium disappears entirely by ~L8 V. However, as stated earlier, the Na I doublet in our spectra does not arise from the ground state and as a higher excitation doublet is expected to weaken at lower temperatures, just as observed. The ground-state Na D doublet, on the other hand, should be investigated even though Burrows & Sharp indicate that sodium forms into NaCl at much lower temperatures than those considered here, around 1150 K.

Moving to later types and cooler temperatures, the next feature to weaken is iron hydride, but this molecule is unfortunately not included in the Burrows & Sharp calculations. Chromium hydride, which is included in the models, follows, and it weakens markedly between types L5 and L8. This suggests that its predicted disappearance at ~1400 K corresponds to a type (yet to be defined) just cooler than L8 V.

The remaining features of L-dwarf spectra—Li I, CO, Rb I, Cs I, K I, and H_2O—are not seen to vanish in the L sequence. Carbon is still predominantly found in carbon monoxide, not methane, so an L8 dwarf must be above 1200–1500 K. Rubidium, cesium, and potassium are all still visible, indicating that they have yet to form their chlorides. This means that an L8 dwarf must be warmer than 1200 K. Finally, water is still present in the optical and near-infrared spectra, not having yet condensed into clouds and dropped

[13] Admittedly though, since VO lacks a sharp band head, its disappearance is a little more difficult to ascertain. However, the ~7950 Å inflection point in the spectrum of late-M and early-L dwarfs is caused by VO, and this inflection has vanished by L4 V.

below the photosphere (as water has apparently done in the atmosphere of Jupiter). However, this occurs at much lower temperatures ($\sim$350 K). Lithium is discussed in detail in § 8.3.

Given the above arguments, we can state that the L-dwarf sequence represents temperatures from somewhere above 2000 K for L0 V down to $\sim$1400 K for L8 V.

However, the use of molecular equilibrium diagnostics is more complicated than simply equating these temperatures to the effective temperature of the star, as illustrated by application of these ideas to Gl 229B with $T_{\rm eff} \approx 950$ K. The fact that Gl 229B shows CO in the near-IR and atomic Cs I lines in the far-optical (Oppenheimer et al. 1998) demonstrates this point. Cesium and carbon monoxide should not exist in this form at this temperature, and the apparent solution is that mixing in the atmosphere of Gl 229B pulls up Cs I and CO from hotter layers below. On the other hand, because the L-dwarf spectral signatures are so well correlated with predictions, this probably means that these objects—unlike Gl 229B and Jupiter—have stable radiative zones.

As a check of our somewhat naive assumptions from above, then, we can compare these results to atmospheric model fits performed on other cool dwarfs having spectroscopy from $\sim$6000 Å to 2.5 μm or beyond. These comparisons are given in Table 12, which lists fits only to models that include grains and/or dust opacities, known to play important roles in determining the emergent spectra of these objects. From these results we can assign a better temperature of $\sim$2000 K to type L0 V based on the slightly warmer temperatures assigned to the late-M dwarfs vB 10 and LHS 2924. The temperature fits to spectra of Kelu-1 and GD 165B are also consistent with the temperatures derived from Table 11. Assigning a temperature to type L8 V is less straightforward, but it must lie between the 1800–1900 K regime of GD 165B and the 900–1000 K regime of Gl 229B. Based on the rapid vanishing (but not total disappearance) of CrH, the correct temperature is probably near 1500 K.

Thus, it is a good first guess that the temperature scale goes from $\sim$2000 K at L0 V to $\sim$1500 K at L8 V. Once we obtain *JHK* spectra of all of the 2MASS L dwarfs, we will rederive the temperature scale based on true fits to synthetic spectra.

8.3. *Substellarity*

An obvious question to ask is, "Are any of these L dwarfs substellar?" Based on the lithium test alone (§ 6.3), we would say that roughly one-third of all known L dwarfs are brown dwarfs. Basri (1998) has shown that any object with lithium absorption and $T_{\rm eff} < 2670$ K is a brown dwarf. Although lithium absorption is a sufficient condition for substellarity in L dwarfs, it is not a necessary one since brown dwarfs more massive than $\sim$0.060 $M_\odot$ are capable of burning their primordial lithium if they are old enough.

There are, however, two potential problems with the lithium test.

1. It assumes that these objects are fully convective so that the elemental constituents of the photosphere are a direct reflection of the elemental constituents of the interior. In other words, any elements present at the surface would have to be those capable of withstanding the temperatures in the core. This assumption may fail if the atmosphere breaks up into radiative zones.

However, brown dwarf research in the Pleiades cluster has proven that this should not be a concern. Results from Stauffer, Schultz, & Kirkpatrick (1998) show that there is a distinct "lithium edge" in the cluster: Pleiades dwarfs with types of M6.5 or earlier show no lithium, whereas those with cooler types do. The fact that lithium depletion shows such an abrupt edge in spectral type provides strong evidence that the coolest Pleiades dwarfs are fully convective and that even at their young ages ($\sim$125 Myr) have had enough time to destroy completely their initial lithium content. Theoretical isochrones show that these young objects fall in the same mass range as the (assumed older) L dwarfs considered here. That is, these are the same objects seen at two different points in their evolutionary history, with the late-M Pleiades dwarfs cooling with time to become L dwarfs.

Turning the argument around, we can say that L dwarfs (at least those of higher mass) share a common history with the late-M Pleiades dwarfs in that they must also have passed through a stage where they were once fully convective *regardless of whether or not they are fully convective now*. While fully convective they would have had sufficient time to destroy their lithium content if core temperatures were high enough. The only L dwarfs not sharing a common history with the late-M Pleiades dwarfs would be extremely low mass objects certain to be brown dwarfs. Thus, even if L dwarfs have begun to form radiative zones, the lithium test should still hold.

2. Searching for lithium at 6708 Å may prove futile below $T_{\rm eff} \approx 1400$ K because atomic lithium will have formed into LiCl (Burrows & Sharp 1999). Although the coolest known L dwarfs are thought to be just warmer than this limit, the disappearance of atomic lithium in cool L dwarfs would provide another useful temperature fiducial. It is interesting to note that we see extremely strong lithium in the spectra of the 2MASS L5.5 and L6 dwarfs, yet there is no lithium in the DENIS L7 dwarf and only a possible detection in the 2MASS L8 dwarf (though this upper limit is not well

TABLE 12

PUBLISHED TEMPERATURES FOR VERY COOL DWARFS AS DERIVED FROM FITS TO SYNTHETIC SPECTRA

Object (1)	Spectral Type (2)	Derived Temperature (K) (3)	Reference (4)
vB 10.....	M8 V	2200	Jones & Tsuji 1997
LHS 2924.....	M9 V	2000–2200	Jones & Tsuji 1997; Tsuji, Ohnaka, & Aoki 1996a
Kelu-1	L2 V	1900	Ruiz et al. 1997
GD 165B	L4 V	1800–1900	Kirkpatrick et al. 1999; Tsuji et al. 1996b
Gl 229B.....	T dwarf	900–1000	Marley et al. 1996; Tsuji et al. 1996b

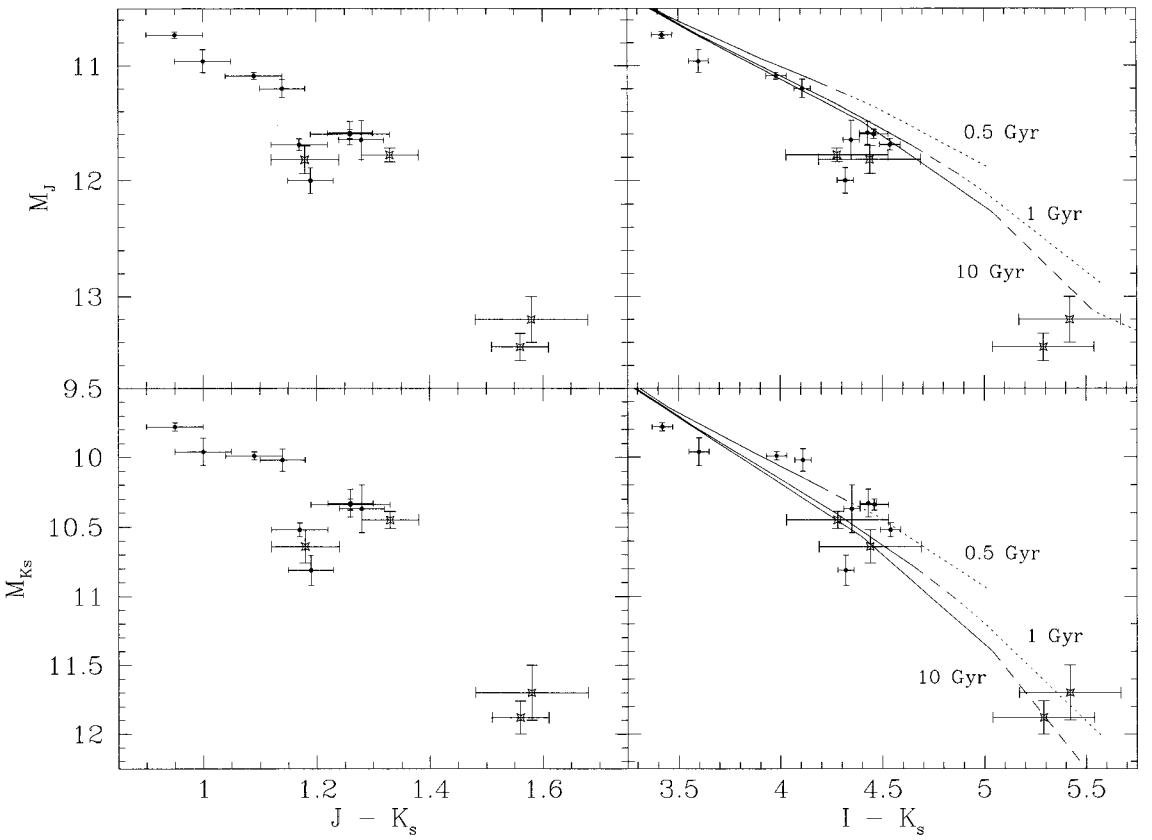

FIG. 18.—Observational H-R diagram for late-M dwarfs (*filled circles*) and the L dwarfs from Table 10 (*open symbols*). Shown on the $I-K_s$ diagrams are the theoretical tracks from Baraffe et al. (1998) for ages of 0.5, 1, and 10 Gyr. Each track consists of a solid line indicating the regime occupied by stars and a short-dashed line indicating the regime occupied by brown dwarfs. The intermediate region (of "transition objects") is shown by a long-dashed line.

constrained). This may mean that a spectral type of ~L7 V corresponds to the LiCl formation temperature of ≤ 1400 K. This assumption needs to be checked via a larger sample, i.e., by checking to see if other yet-to-be-discovered dwarfs of type L7 or later also show no lithium absorption at 6708 Å. Better yet, checking for the onset of LiCl absorption in the infrared would be an even more direct check.

It should be noted the signal-to-noise ratio and resolution of our LRIS observations are not sufficient to identify the Li line in all spectra (see Fig. 15*b*), so there may be other L dwarfs in our sample that do pass the lithium test. Furthermore, any objects in the sample cooler than ~1400 K may not show lithium absorption either, since lithium will have formed into LiCl. These arguments therefore suggest that the lithium test as performed on our spectra provides only a lower bound to the number of brown dwarfs contained in our sample. Based on the number that show lithium absorption, then, we can claim that *at least one-third* of all known L dwarfs are substellar.

We can make other checks on the substellarity independent of the lithium test, too. Figure 18 shows the observational H-R diagram for the L dwarfs and some late-M dwarfs with trigonometric parallax measures. Also plotted are theoretical models from Baraffe et al. (1998).[14] The models show that for an age of 1 Gyr, mid- to late-L dwarfs are all substellar; at much larger ages (10 Gyr), the earliest L dwarfs are stellar, with the later L dwarfs being comprised of transition objects and brown dwarfs. These results agree qualitatively with those from the lithium test.

Another check on substellarity can be made by comparing the effective temperatures of these objects (from the molecular equilibrium analysis of § 8.2) to the predictions of model interiors. The effective temperature as a function of time is shown in Figure 19 for a variety of masses from 0.010 to 0.100 $M_\odot$. In the top panel of the figure are shown the latest models of Burrows et al. (1997), and in the bottom panel those of Baraffe et al. (1998). Indicated by the thick horizontal lines on each panel is the approximate temperature range spanned by L dwarfs. According to the Burrows et al. models, the lowest mass stars (~0.078 $M_\odot$) eventually stabilize at a temperature near 1750 K (shown by the dashed line). This dividing line lands squarely in the middle of the L-dwarf temperature range, meaning that the latest L dwarfs are all substellar and the earlier ones represent a mixture of stars and brown dwarfs. Note that brown dwarfs can exist at the earliest L types with ages as old as 2 Gyr. According to the Baraffe et al. models, the lowest mass stars (~0.075 $M_\odot$) stabilize at temperatures near 2000 K, meaning that the entire L sequence is "sub"-stellar. However, objects with masses between 0.072 and 0.075 $M_\odot$ may stabilize after more than a Hubble time at a temperature near 1700 K. In this case, the latest L dwarfs are all brown dwarfs with earlier types representing a mixture of brown dwarfs and "transition objects."

All checks therefore agree that a substantial fraction of L dwarfs are brown dwarfs. Atmospheric modeling that includes the effects of grain depletion and grain opacities is now being developed, and once it accurately reproduces

[14] These models do not yet incorporate grains and fail to predict the red $J-K_s$ colors seen for L dwarfs. As a result, models are overplotted only for the $I-K_s$ diagrams, where the agreement is reasonable.

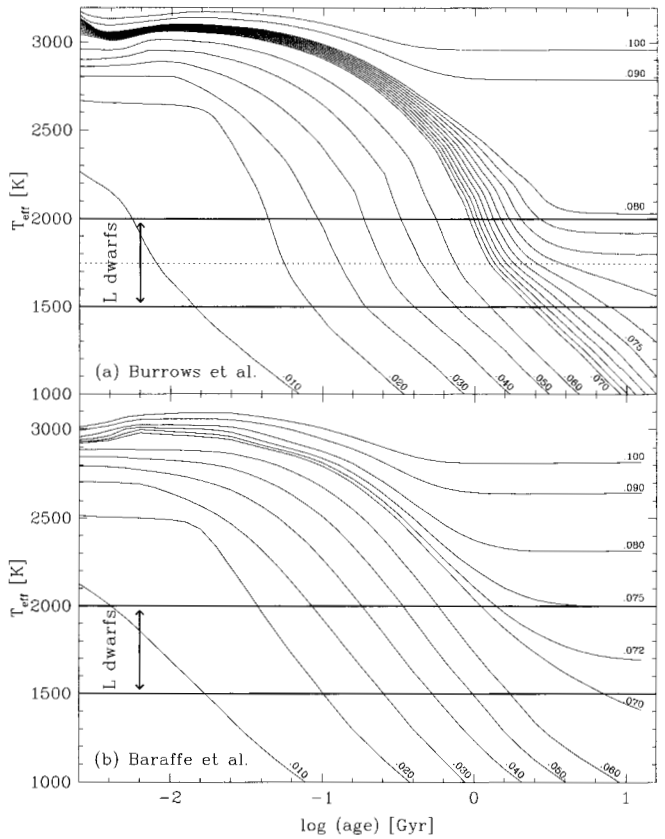

FIG. 19.—Tracks of T_{eff} vs. age as predicted by the models of (*a*) Burrows et al. (1997) and (*b*) Baraffe et al. (1998). The mass, in $M_{\odot}$, is shown along each track. (The unlabeled tracks between 0.070 and 0.080 $M_{\odot}$ in (*a*) are 0.001 $M_{\odot}$ subdivisions, plotted to better highlight the break point between stars and brown dwarfs.) The approximate temperature regime spanned by L dwarfs (1500–2000 K) is shown by the thick horizontal lines. In (*a*), the minimum temperature attained by stellar objects is shown by the dashed line.

colors and observed spectra of L dwarfs, we will have a much better understanding of the exact makeup of the L-dwarf classes. Another excellent diagnostic can be obtained for close binary systems with one or more L-dwarf components—here, dynamical masses can be determined and used as additional checks against the theory. In this regard, closer scrutiny of the L dwarfs so far discovered is certainly warranted.

8.4. *Luminosity and Mass Functions for L Dwarfs*

Using the statistics quoted in § 3 along with the absolute magnitudes given in Table 10, we can obtain a preliminary luminosity function (LF) for L dwarfs. Converting this LF into a mass function (MF) is a very difficult undertaking because any given L type represents a range of masses at different ages. Observationally, we cannot obtain either the mass or the age for an isolated L dwarf, so the computation must involve our observational statistics on Li detections (to assign an age spread) and theoretical isochrones (to assign mass spreads). In fact, for the L dwarfs that are substellar, the L spectral sequence represents an evolutionary sequence in which the objects cool to later L (and T) types with advancing age.

These computations are complex and beyond the scope of this paper. Please refer to the companion paper by Reid et al. (1999a) for a full discussion of our derived MF.

9. CONCLUSIONS

Using 371 deg^2 of 2MASS data, we have obtained spectroscopic classifications of 51 objects with no optical counterparts. A large fraction of these were found to be dwarfs cooler than the coolest known M dwarf with spectra lacking the familiar oxide bands of M stars. We have placed these new objects into a new spectral class called "L." We have presented criteria defining this new class and have established a recipe for the spectral classification of other L dwarfs using a grid of objects set aside as spectral standards. We have shown that several of the L dwarfs known show Li I absorption, indicating that at least one-third of all L dwarfs are brown dwarfs. We have also given a qualitative description of the atmospheric physics using a marriage of observation with theory and have made a first attempt at determining the effective temperature scale for the L sequence.

J. D. K. thanks Phil Keenan, Bill Bidelman, Pat Boeshaar, Chris Corbally, Bob Garrison, and Richard Gray for their wisdom and advice concerning the definition of a new spectral class. The referee, Pat Boeshaar, made several insightful suggestions, which helped with the physical interpretation of these spectra. The authors also thank Sandy Leggett and Tom Kerr for help in obtaining the *K*-band spectra from UKIRT, Rik Williams for his help in producing the finder charts in Figure 2, Adam Burgasser for his comments on the final version of the manuscript, Ben Oppenheimer for use of some of the spectra in his Gl 229B library, George Djorgovski for an early confirmation spectrum of the L dwarf 2MASSW J1439284+192915, and John B. Hearnshaw for his fantastic book (Hearnshaw 1986) on the history of stellar spectral classification. We thank Adam Burrows and the rest of the Burrows et al. (1997) team for making the tabular data of their models available for use in Figure 19. We also thank Isabelle Baraffe, Gilles Chabrier, and the rest of the Baraffe et al. (1998) team for making the tabular data of their models available for use in Figures 18 and 19. J. D. K., I. N. R., and J. L. acknowledge funding through a NASA/JPL grant to 2MASS Core Project science. J. D. K., R. M. C., B. N., and C. A. B. acknowledge the support of the Jet Propulsion Laboratory, California Institute of Technology, which is operated under contract with the National Aeronautics and Space Administration. The new trigonometric parallaxes reported in Table 10 are being carried out as part of the regular CCD parallax program at the US Naval Observatory in Flagstaff, Arizona. We thank the other members of the USNO team who have contributed to the observations: Harry Guetter, Hugh Harris, Chris Luginbuhl, Alice Monet, Ron Stone, and Dick Walker. The *K*-band spectra of Figure 5 were obtained as part of the UKIRT Service Programme. The United Kingdom Infrared Telescope is operated by the Joint Astronomy Centre on behalf of the UK Particle Physics and Astronomy Research Council. The finder charts of Figure 2 make use of the Digitized Sky Survey, which was produced at the Space Telescope Science Institute under US Government grant NAGW-2166. Research in this paper has also relied partly on photographic plates obtained at the Palomar Observatory 48 inch (1.2 m) Oschin Telescope for the Second Palomar Observatory Sky Survey, which was funded by the Eastman Kodak Company, the National Geographic Society, the Samuel

Oschin Foundation, the Alfred Sloan Foundation, the National Science Foundation grants AST 84-08225, AST 87-19465, AST 90-23115, and AST 93-18984, and the National Aeronautics and Space Administration grants NGL 05002140 and NAGW 1710. This research has also made use of the SIMBAD database, operated at CDS, Strasbourg, France. This publication makes use of data from the 2-Micron All-Sky Survey, which is a joint project of the University of Massachusetts and the Infrared Processing and Analysis Center, funded by the National Aeronautics and Space Administration and the National Science Foundation.

APPENDIX A

NOTES ON INDIVIDUAL L DWARFS

Several of the L dwarfs in Table 3 are worthy of special mention.

2MASP J0345432+254023 (L0 V).—This object, discovered in data taken by the 2MASS Prototype Camera, was first announced in Kirkpatrick et al. (1997a). At that time, it was given a provisional spectral type of ≥M10 V. The quality of our Keck spectrum greatly exceeds that of the Palomar spectrum published in that paper. The USNO parallax (Table 10) places it at 28.2 pc.

2MASSW J0147334+345311 (L0.5 V).—This object is a close double at separation of ~2″, but the spectrum of the second object shows it to be a background M star.

2MASSW J1439284+192915 (L1 V).—The very high proper motion of this object was first seen as an obvious positional offset between the POSS-II III-F and IV-N plates taken only 4 yr apart. Extrapolating this motion back to the epoch of the POSS-I plate shows the 2MASS object at an R magnitude of 19.0 as measured by the Automated Plate Measuring (APM) facility, thus yielding a color of $R_{\rm APM}-K_s=7.7$. The motion computed by the USNO (Table 10) is $\mu = 1\farcs30\ {\rm yr}^{-1}$ at $\theta = 289°$, and the resulting parallax places it at 15.1 pc.

2MASSW J1439409+182637 (L1 V).—This is the warmest L dwarf showing a discernible lithium line (EW = 5.6 Å). Two warmer field objects, SERC-296A (type M6 V; Thackrah, Jones, & Hawkins 1997) and LP 944−20 (type M9 V; Tinney 1998), also show lithium. The former may just be a very young star; both LP 944−20 and 2MASSW J1439409+182637, however, are so low in temperature that they could not be anything but brown dwarfs.

Kelu-1 (L2 V).—Discovered by Ruiz et al. (1997), our spectrum shows a very weak lithium line (EW = 1.7 Å) and very weak Hα emission (EW = 1.9 Å). 2MASS has also scanned this object, which carries the additional designation 2MASSW J1305402−254106.

2MASSW J1342236+175156 (L2.5 V).—There is a background galaxy located ~5″ to the west of this L dwarf. There may be a lithium line just at the limit of our detection (EW = 3.9 Å).

2MASSW J1146345+223053 (L3 V).—This object shows a strong lithium line with an EW of 5.1 Å. This object is also a close double with separation of ~1″ at P.A. = 315°. Our LRIS spectrum shows that the other component is a background star of much earlier type.

DENIS-P J1058.7−1548 (L3 V).—Discovered by Delfosse et al. (1997), our spectrum shows weak Hα emission with EW of 1.6 Å. This object has also been scanned by 2MASS and carries the additional designation 2MASSW J1058479−154817. The coordinates encrypted into the 2MASS designation are accurate to <0.″5 with respect to the *Hipparcos/Tycho* reference frame, a vast improvement over the coordinates given in Delfosse et al. (1997).

2MASSW J0326137+295015 (L3.5 V).—This object, located in projection against more distant molecular cloud complexes in Perseus, has the strongest Hα emission line seen in any L dwarf (EW = 9.1 Å).

2MASSW J0129122+351758 (L4 V).—This object has a clear lithium line with an EW of 3.3 Å.

GD 165B (L4 V).—The prototype of the L-dwarf class (Kirkpatrick, Henry, & Liebert 1993), this object was discovered by Becklin & Zuckerman (1988) as the companion to a white dwarf. The separation between components is 4″. See Kirkpatrick et al. (1999) for a current review of this object.

DENIS-P J1228.2−1547 (L5 V).—Discovered by Delfosse et al. (1997) and later shown to have lithium by Tinney et al. (1997) and Martín et al. (1997), this object shows a lithium line with an EW of 3.1 Å in our spectrum. The object has also been rediscovered in 2MASS data from the southern hemisphere, where it carries the designation of 2MASSW J1228152−154734. The position encoded into this designation is more accurate than the position provided by Delfosse et al. (1997).

2MASSW J1553214+210907 (L5.5 V).—This object shows the strongest lithium line ever seen in a brown dwarf: the EW is 18.5 Å.

2MASSs J0850359+105716 (L6 V).—This object also shows a remarkably strong lithium line with an EW of 15.2 Å. The LRIS guider camera at Keck shows a second component, with separation of <2″ at P.A. = 82°, but the spectrum confirms that this secondary is a background M dwarf. The K-band spectrum of the brown dwarf (Fig. 5) shows clear CO absorption and strong H_2O bands.

DENIS-P J0205.4−1159 (L7 V).—Also discovered by Delfosse et al. (1997), this object has been scanned by 2MASS where it carries the designation 2MASSW J0205293−115930. The USNO parallax places it at 16.6 pc.

2MASSW J1632291+190441 (L8 V).—This is the coolest L dwarf currently known, and it shows a possible lithium line at our detection limit (EW ≤ 9.4 Å). The spectrum is quite smooth throughout the far-optical region and shows weak CrH and even weaker FeH bands. The only other obvious molecular absorption is H_2O near 9300 Å. Lines of the alkali metals are still present with Na I exceedingly weak, K I extremely broadened, and Rb I and Cs I very strong. The near-infrared spectrum (Fig. 5) shows a distinct CO band head and strong absorption by H_2O.

Gl 229B (T dwarf).—Located 7".7 away from the M1 dwarf Gl 229A, this object was discovered by Nakajima et al. (1995). Like 2MASSW J1632291+190441, this object shows strong Cs I lines and a strong H_2O band (Fig. 7), but in Gl 229B the hydrides have completely disappeared. Despite similarities in the far-optical region, though, the *K*-band spectra (Fig. 5) show pronounced differences, with 2MASSW J1632291+190441 exhibiting weak CO bands and Gl 229B showing strong absorption by CH_4.

APPENDIX B

NOTES ON OTHER OBJECTS

Several of the non–L-dwarf objects listed in Tables 1A and 2 are worthy of special mention. Fifteen of these are ultracool M dwarfs (type M7 V or cooler). Distance estimates for these are listed in Table 13. Notes on individual objects of interest are given below.

2MASSW J0149090+295613 (M9.5 V).—An inspection of the POSS-I and POSS-II plates of the region revealed that this is a high proper-motion star with $\mu = 0''.51\ \mathrm{yr}^{-1}$ at P.A. = 156°. (As such, it does not strictly belong in the sample since it has a POSS-I E-plate counterpart—any nonmotion object with identical magnitudes and colors would not have been chosen.) Despite its large motion, it was not detected by the proper-motion surveys of Luyten (1979b, 1980) because it is within a few arcseconds of a brighter star at the epoch of the POSS-I survey and because it is invisible on the POSS-I O plate. Our first follow-up observations on 1997 December 7 (UT) showed an object with a rich, time-variable spectrum of very strong emission lines. In particular, the equivalent width (EW) of the Hα line was >300 Å. Subsequent observations of the object on 1997 December 24 (UT) from the Palomar 5 m telescope along with additional Keck observations on 1998 January 22, 23, and 24 (UT) showed an object with the spectrum of a "normal" M9.5 dwarf. In these quiescent spectra, only the Hα line is still seen in emission, and then at a mere ~10 Å EW. Its estimated distance is 21 pc. See the companion paper by Liebert et al. (1999a) for more on this intriguing object.

2MASSW J0244463+153531 (M5 V + M5.5 V).—This is a close (~2") double M dwarf.

2MASP J0348036+234411 (M7.5 V).—This is an ultracool M dwarf at an estimated distance of 46 pc. This object has been announced as a possible Pleiades brown dwarf and named "NOT 1" by Festin (1997, 1998) who, to make it consistent with Pleiades membership, suggests that the object is an equal-magnitude binary. We suggest, however, that it is merely a foreground object.

2MASSW J0401096+182808 (carbon star).—This is a carbon star as identified by weak bands of CN throughout its far-optical spectrum. It is an unusual carbon star, however, in that it shows emission lines of K I, Rb I, and Cs I along with a broad unidentified feature near 8800 Å. For a discussion of this object, see the companion paper by Liebert et al. (1999b).

2MASSs J0857258+172052 (carbon star).—This is a high-latitude carbon star first identified from the *IRAS* survey and dubbed IRAS SSC 08546+1732 (Cutri et al. 1989). A comparison of this object to the unusual carbon star mentioned above can also be found in Liebert et al. (1999b).

2MASSW J0921457+191812 (QSO).—This object was selected by both the 2MASS brown dwarf search and the 2MASS QSO search. Its spectrum shows that it is a QSO at $z = 1.8$. Details can be found in the companion papers by Cutri et al. (1999) and Nelson et al. (1999).

TABLE 13

ULTRACOOL M DWARFS FROM TABLES 1A AND 2

Object Name (1)	Spectral Type (2)	*J* (3)	*H* (4)	K_s (5)	Estimated Distance (pc) (6)
2MASSW J0010037+343610.....	M8 V	15.66 ± 0.07	15.08 ± 0.09	14.38 ± 0.07	82
2MASSW J0055384+275652.....	M7 V	15.73 ± 0.07	14.86 ± 0.07	14.46 ± 0.08	94
2MASP J0147362+365855	M7 V	14.8 ± 0.1	14.2 ± 0.1	13.6 ± 0.1	65
2MASSW J0149090+295613.....	M9.5 V	13.42 ± 0.03	12.57 ± 0.04	12.00 ± 0.03	21
2MASSs J0251222+252124	M9 V	15.89 ± 0.07	14.97 ± 0.07	14.40 ± 0.07	67
2MASSs J0251253+262504	M9 V	16.00 ± 0.08	15.22 ± 0.09	14.51 ± 0.07	73
2MASP J0348036+234411	M7.5 V	14.27 ± 0.04	13.64 ± 0.05	13.23 ± 0.04	46
2MASSW J0914188+223813.....	M9.5 V	15.30 ± 0.05	14.40 ± 0.05	13.90 ± 0.04	51
2MASSW J1214063+202702.....	M7 V	15.67 ± 0.07	15.08 ± 0.08	14.45 ± 0.11	97
2MASSW J1239194+202952.....	M9 V	14.48 ± 0.04	13.65 ± 0.04	13.16 ± 0.04	36
2MASSW J1434264+194050.....	M8 V	15.55 ± 0.06	14.83 ± 0.09	14.39 ± 0.11	76
2MASSW J1710255+210715.....	M8 V	15.87 ± 0.08	15.02 ± 0.09	14.46 ± 0.11	85
2MASSW J2258066+154416.....	M7.5 V	16.18 ± 0.09	15.35 ± 0.11	14.71 ± 0.12	107
2MASSW J2258590+152047.....	M7 V	15.59 ± 0.06	15.02 ± 0.07	14.59 ± 0.10	94
2MASSW J2309462+154905.....	M8.5 V	15.01 ± 0.06	14.34 ± 0.06	13.91 ± 0.07	53

REFERENCES

Allard, F. 1990, Ph.D. thesis, Univ. Heidelberg
Anders, E., & Grevesse, N. 1989, Geochim. Cosmochim. Acta, 53, 197
Baraffe, I., Chabrier, G., Allard, F., & Hauschildt, P. H. 1998, A&A, 337, 403
Basri, G. 1998, in ASP Conf. Ser. 134, Brown Dwarfs and Extrasolar Planets, ed. R. Rebolo, E. L. Martín, & M. R. Zapatero Osorio (San Francisco: ASP), 394
Becklin, E. E., & Zuckerman, B. 1988, Nature, 336, 656
Berriman, G., & Reid, N. 1987, MNRAS, 227, 315
Bessell, M. S. 1979, PASP, 91, 589
———. 1991, AJ, 101, 662
Bessell, M. S., & Brett, J. M. 1988, PASP, 100, 1134
Boeshaar, P. C., & Tyson, J. A. 1985, AJ, 90, 817
Bouigue, R. 1954, Ann. d'Astrophys., 17, 104
Burrows, A., & Liebert, J. 1993, Rev. Mod. Phys., 65, 301
Burrows, A., & Sharp, C. M. 1999, ApJ, 512, 843
Burrows, A., et al. 1997, ApJ, 491, 856
Cannon, A. J., & Pickering, E. C. 1901, Ann. Astron. Obs. Harvard Coll., 28(II), 131
———. 1923, Ann. Astron. Obs. Harvard Coll., 98, 1
Cutri, R. M., Low, F. J., Kleinmann, S. G., Olszewski, E. W., Willner, S. P., Campbell, B., & Gillett, F. C. 1989, AJ, 97, 866
Cutri, R. M., Nelson, B. O., Kirkpatrick, J. D., Lonsdale, C. J., Beichman, C. A., Huchra, J. P., & Skrutskie, M. F. 1999, in preparation
Delfosse, X., et al. 1997, A&A, 327, L25
Festin, L. 1997, A&A, 322, 455
———. 1998, A&A, 333, 497
Geballe, T. R., Kulkarni, S. R., Woodward, C. E., & Sloan, G. C. 1996, ApJ, 467, L101
Gliese, W., & Jahreiss, H. 1991, Astronomical Data Center CD-ROM: Selected Astronomical Catalogs, Vol. 1, ed. L. E. Bratzmann & S. E. Gesser (Greenbelt, MD: NASA/GSFC)
Golimowski, D. A., Burrows, C. J., Kulkarni, S. R., Oppenheimer, B. R., & Brukardt, R. A. 1998, AJ, 115, 2579
Gordon, C. P. 1971, PASP, 83, 667
Hamuy, M., Suntzeff, N. B., Heathcote, S. R., Walker, A. R., Gigoux, P., & Phillips, M. M. 1994, PASP, 106, 566
Hearnshaw, J. B. 1986, The Analysis of Starlight: One Hundred Years of Astronomical Spectroscopy (New York: Cambridge Univ. Press)
Jones, H. R. A., & Tsuji, T. 1997, ApJ, 480, L39
Keenan, P. C., & Morgan, W. W. 1941, ApJ, 94, 501
Kirkpatrick, J. D. 1994, in The Bottom of the Main Sequence—and Beyond, ed. C. G. Tinney (Heidelberg: Springer), 140
———. 1998, in ASP Conf. Ser. 134, Brown Dwarfs and Extrasolar Planets, ed. R. Rebolo, E. Martín, & M. R. Zapatero-Osorio (San Francisco: ASP), 405
Kirkpatrick, J. D., Allard, F., Bida, T., Zuckerman, B., Becklin, E. E., Chabrier, G., & Baraffe, I. 1999, ApJ, 519, 834
Kirkpatrick, J. D., Beichman, C. A., & Skrutskie, M. F. 1997a, ApJ, 476, 311
Kirkpatrick, J. D., Henry, T. J., & Irwin, M. J. 1997b, AJ, 113, 1421
Kirkpatrick, J. D., Henry, T. J., & Liebert, J. 1993, ApJ, 406, 701
Kirkpatrick, J. D., Henry, T. J., & McCarthy, D. W., Jr. 1991, ApJS, 77, 417
Kirkpatrick, J. D., Henry, T. J., & Simons, D. A. 1995, AJ, 109, 797
Leggett, S. K. 1992, ApJS, 82, 351
Liebert, J., Kirkpatrick, J. D., Reid, I. N., & Fisher, M. D. 1999a, ApJ, in press
Liebert, J., et al. 1999b, in preparation
Luyten, W. J. 1979a, LHS Catalog (Minneapolis: Univ. Minnesota Press)
———. 1979b, NLTT Catalogue, Vol. I–II (Minneapolis: Univ. Minnesota)
———. 1980, NLTT Catalogue, Vol. III–IV (Minneapolis: Univ. Minnesota)
Marley, M. S., Saumon, D., Guillot, T., Freedom, R. S., Hubbard, W. B., Burrows, A., & Lunine, J. I. 1996, Science, 272, 1919
Martín, E. L., Basri, G., Delfosse, X., & Forveille, T. 1997, A&A, 327, L29
Monet, D. G., Dahn, C. C., Vrba, F. J., Harris, H. C., Pier, J. R., Luginbuhl, C. B., & Ables, H. D. 1992, AJ, 103, 638
Morgan, W. W., Keenan, P. C., & Kellman, E. 1943, An Atlas of Stellar Spectra, with an Outline of Spectral Classification (Chicago: Univ. Chicago Press)
Nakajima, T., Oppenheimer, B. R., Kulkarni, S. R., Golimowski, D. A., Matthews, K., & Durrance, S. T. 1995, Nature, 378, 463
Nelson, B. O., Cutri, R. M., Kirkpatrick, J. D., Neugebauer, G. X., & Skrutskie, M. F. 1999, in preparation
Oke, J. B., et al. 1995, PASP, 107, 375
Oppenheimer, B. R., Kulkarni, S. R., Matthews, K., & van Kerkwijk, M. H. 1998, ApJ, 502, 932
Persson, S. E., Murphy, D. C., Krzeminski, W., Roth, M., & Reike, M. J. 1998, AJ, 116, 2475
Pickering, E. C. 1890, Ann. Astron. Obs. Harvard Coll., 27, 1
———. 1908, Circ. Harvard Coll. Obs. 145
Reid, I. N., et al. 1999a, ApJ, submitted
———. 1999b, in preparation
Ruiz, M. T., Leggett, S. K., & Allard, F. 1997, ApJ, 491, L107
Secchi, A. 1866, CR Acad. Sci. Paris, 63, 621
Skrutskie, M. F., et al. 1997, The Impact of Large-Scale Near-IR Sky Surveys, ed. F. Garzon et al. (Dordrecht: Kluwer), 25
Stauffer, J. R., Schultz, G., & Kirkpatrick, J. D. 1998, ApJ, 499, L199
Thackrah, A., Jones, H., & Hawkins, M. 1997, MNRAS, 284, 507
Tinney, C. G. 1998, MNRAS, 296, L42
Tinney. C. G., Delfosse, X., & Forveille, T. 1997, ApJ, 490, L95
Tinney, C. G., Delfosse, X., Forveille, T., & Allard, F. 1998, A&A, 338, 1066
Tinney, C. G., Mould, J. R., & Reid, I. N. 1993, AJ, 105, 1045
Tsuji, T., Ohnaka, K., & Aoki, W. 1996a, A&A, 305, L1
Tsuji, T., Ohnaka, K., Aoki, W., & Nakajima, T. 1996b, A&A, 308, L29
van Altena, W. F., Lee, J. T., & Hoffleit, E. D. 1995, The General Catalogue of Trigonometric Stellar Parallaxes (4th ed.; Schenectady: Davis)